Sediment Transport Dynamism in the Confluence Area of Two Rivers Transporting Mainly Suspended Sediment Based on Sentinel-2 Satellite Images

Ahmed Mohsen [1,2,*], Ferenc Kovács [1], Gábor Mezősi [1] and Tímea Kiss [1]

[1] Department of Geoinformatics, Physical and Environmental Geography, University of Szeged, Egyetem u. 2–6, 6722 Szeged, Hungary; kovacsf@geo.u-szeged.hu (F.K.); mezosi@geo.u-szeged.hu (G.M.); kisstimi@gmail.com (T.K.)

[2] Department of Irrigation and Hydraulics Engineering, Tanta University, Tanta 31527, Egypt

[*] Correspondence: ahmed_mohsen250@f-eng.tanta.edu.eg

Abstract: Downstream of the confluence of rivers, complex hydrological and morphological processes control the flow and sediment transport. This study aimed to analyze the spatio-temporal dynamics of suspended sediment in the confluence area of the Tisza and its main tributary Maros River using Sentinel-2 images and to reveal the correlation between the hydrological parameters and the mixing process through a relatively long period (2015–2021). The surficial suspended sediment dynamism was analyzed by applying K-means unsupervised classification algorithm on 143 images. The percentages of the Tisza (TW) and Maros (MW) waters and their mixture (MIX) were calculated and compared with the hydrological parameters in both rivers. The main results revealed that the areal, lateral, and longitudinal extensions of TW and MIX have a better correlation with the hydrological parameters than the MW. The Pearson correlation matrix revealed that the discharge ratio between the rivers controls the mixing process significantly. Altogether, 11 mixing patterns were identified in the confluence area throughout the studied period. The TW usually dominates the confluence in November and January, MW in June and July, and MIX in August and September. Predictive equations for the areal distribution of the three classes were derived to support future water sampling in the confluence area.

Keywords: stream junctions; remote sensing; hydrological parameters; sediment load; mixing of tributaries

1. Introduction

River confluences are one of the most essential geomorphological spots along rivers, as they control the flow and sediment transport conditions downstream [1]. The confluences can form in various hydro-morphological configurations. The most common is when a smaller tributary joins a mainstream with higher discharge, but two similar streams can also join to form a new river. However, when two side-channels are separated by an island and re-join at the end of the island, this also creates a confluence [2].

The hydrodynamics in the confluence area is complex, and it has a spatio-temporal variability. This complexity arises from the various parameters (e.g., water slope, velocity, discharge, momentum, and geomorphological characteristics) of the joining rivers, controlling the water and sediment transport process [3,4]. The transferred momentum from the tributary and the water circulation in the confluence area increases the probability of scour hole formation, which could alter river morphology [5]. Similarly, the turbulence intensity in the confluence area plays a key role in sediment transport and the mixing of various pollutants, which affects the water quality conditions downstream [4]. Therefore, the sampling process of any water constituents in a confluence should be performed only

if the actual mixing situation is identified, as various mixing can highly influence the results. Very often, the fluviometers (gauging stations) are in towns located near to confluences; thus, studying the mixing patterns and process in confluences is a crucial issue to avoid misrepresentation of the collected data.

The local flow and sediment regimes in the confluence area are influenced considerably by the geometrical characteristics of the joining streams and in particular, the confluence angle and bed discordance [1,6]. The confluence area could be divided into six different zones [6]. (1) The stagnation zone is formed at the upstream corner of the confluence due to the deflection of flows. (2) The flow deflection zone is formed as the result of the induction of the tributary and main steam waters into the confluence. This zone is correlated to the stagnation zone, and it increases with higher confluence angel and/or higher discharge ratio between the tributary and the main stream. (3) The flow separation zone is an area of low-pressure formed at the downstream corner of the confluence [7], though Ashmore et al. [8] argued that in natural confluences, this zone does not exist due to the gradual changing direction of banks. (4) The maximum velocity zone forms due to the confinement of the discharges of the joining streams into a smaller cross-sectional area [1,9]. (5) The recovery zone is located several kilometers downstream of the flow separation zone, where the flow conditions are no longer influenced by the confluence's dynamism. (6) The zone of shear layers develops as the result of water mixing, which stimulates the turbulent mixing of water [10]. The presence of shear layers is considered as a sign of the existence of flow with different velocities parallel to each other [1], triggering the formation of eddies. These eddies are the main driving factors of water and sediment mixing in the confluence zone.

The areal distribution of each zone depends on the morphological and geometrical characteristics of the joining streams (e.g., bed discordance, confluence angle, planform, and the vertical characteristics of the rivers). Best and Reid [11] modelled the dynamism of the separation zone, revealing a strong positive correlation between the dimensions of the separation zone and discharge ratio, particularly at higher confluence angles (70° and 90°). Additionally, the relative velocity, discharge, and momentum between a tributary and a mainstream were also reported as driving factors for the area of each zone and consequently the dominancy of a stream in the confluence area and the mixing process [12–14].

Only a few studies analysed the bedload and suspended transport processes in the confluence zones due to the difficulties of their measurement in turbulent flows [4,6,15–18]. Best [19] claimed that the bed load transported by the joining streams could be distinguished clearly, as they appear at both sides of the scour zone, while a very modest amount moves to the scour zone itself. On the other hand, Roy and Bergeron [16] disclosed a contrary behaviour, as the marked particles were mixed towards the scour zone without any segregation. Those studies, which analysed the suspended sediment transport at confluences, usually focused on the mixing rates of the joining rivers [19–21]. In many confluences, the mixing process is detectable based on the contrast between the water colour of the joining rivers. The water colour depends mainly on catchment characteristics (e.g., geological setting, runoff, vegetation type, and coverage, and human activities), as well as sediment yield, dissolved chemicals, and biological activity along the river [22,23]. However, Rice et al. [2] proved that the mixing process of suspended and dissolved materials at confluences does not depend on the magnitude of the streams.

The different water colours of the mixing waters could be exploited during the analysis of the mixing patterns in the confluence area. The suspended sediment transport, which is considered as one of the most important parameters for studying the mixing process, could be analysed by in situ campaigns [24,25], modelling [26,27], and remote sensing images [28–39]. As there is a great difference in suspended sediment transport during flood periods, a combination of linear and power models was developed to accommodate all the spectra of suspended sediment from dilute to hyper-concentrated levels [26]. Guyot et al. [24] analyzed the suspended sediment concentration in the confluence

area of the Negro and Solimões Rivers (Brazil) by collecting water samples from nine cross sections. The results revealed that the Solimões River supplied 96.5% of the suspended load. Their longitudinal mixing was studied using a mass balance technique and the results showed that the water mixing extended up to 25 km downstream [40]. Lane et al. [41] modelled the mixing pattern of two large rivers in Argentina (Río Paraná and Río Paraguay), revealing that the complete mixing often takes very long distances in large rivers. However, mixing can also be a rapid process, as it is driven by the momentum ratio between streams, bed discordance, and the formation of water circulation in the confluence area. Jirka [21] concluded that the complete vertical mixing is a quick process, as it could extend longitudinally to a few decades of water depth at maximum. However, lateral mixing requires long distances: for instance, at rivers with a 10–1000 width-depth ratio, a distance of 100–1000 the river`s width is required for complete mixing. On the other hand, lateral mixing could happen faster in discordant bed confluences, in ca. 25 times channel width [42].

The difficulty of in situ assessment of the mixing process at a confluence area is due to the navigation hardships, water turbulence, long mixing distances downstream, and being time consuming. However, remote sensing provides a cost-effective alternative for monitoring suspended sediment or chlorophyll-a [28–37], especially with the current development of the spatial, spectral, and temporal resolutions of the satellite constellations of [43–45]. The general theory of this technique is that the incident light on the water surface takes several actions (scattering, absorption, reflection, or transmission through the water), which depend on the wavelength and the concentrations of water constituents (e.g., suspended sediment). Thus, it could be exploited to predict the suspended load of rivers. Gernez et al. [38] proposed a multi-sensor approach, which can be applied to derive a wide range of suspended sediment concentrations, based on the validation of SPM algorithms developed by Doxaran et al. [46]. The validation process was applied on SPOT and Landsat images for the Gironde and Loire estuaries; however, it could also be applied on any other high spatial resolution sensors such as the Sentinel-2. Umar et al. [47] assessed the longitudinal mixing distance downstream the confluence of the Mississippi and Missouri Rivers, using Landsat-5 TM satellite images and mixing metrics. Marinho et al. [48] investigated the surficial suspended sediment using MODIS satellite images in the confluence of the Solimões and Negro Rivers (Brazil) for one hydrological year; then, they created a model to predict the spatio-temporal mixing pattern of surficial suspended sediment in the confluence area. The research revealed the temporal variations of the mixing, as the Solimões water was dominant in January and February along both banks of the river, however in June and July, the waters hardly mixed. Park et al. [49] studied the spatio-temporal mixing pattern of the Solimões and Negro Rivers too, comparing three different years representing three different hydrological conditions from drought through to an average hydrological condition to flood. The results demonstrated that Amazonian surface water has the highest domination during rising or high-water discharges. Furthermore, the mixing process depends on the hydrological regime as the highest mixing rate took place during flood, and it was followed by the drought and average hydrological regimes.

The previous studies mainly focused on evaluating the longitudinal mixing of the waters until reaching complete mixing [40]. Only a few of them studied the temporal mixing pattern, and they studied only a limited period, e.g., one hydrological year [48] or three years representing various hydrological regimes [49]. Additionally, no study assessed the direct correlation between hydrological parameters (e.g., water stage, water slope and discharge) and the spatio-temporal mixing over a relatively long period of time using satellite images. The previous studies created their suspended sediment models based on supervised learning, which requires the availability of suspended sediment in situ measurements, but no study applied the unsupervised learning approach, which may be useful for remote and isolated confluences.

Therefore, the general aim of this study is to investigate the multi-year spatio-temporal dynamism of the mixing of two rivers using Sentinel-2 satellite images. The confluence of the Tisza and Maros Rivers (Hungary) was selected as a study area as the two rivers transport a considerable amount of suspended sediment, and they can influence each other significantly during floods by impoundment. Therefore, it was hypothesized, that the mixing of the waters depends on the actual hydrological parameters of the two joining rivers. The goals of the research were: (1) to map the spatial distribution of surficial suspended sediment in the confluence area; (2) to identify the driving hydrological factors which affect the spatial characteristics of the mixing water; (3) to identify mixing patterns based on their lateral and longitudinal characteristics; (4) to derive predictive equations of the areal and longitudinal distribution and mixing of the waters of the two rivers based on the hydrological parameters; and (5) to identify those zones in the confluence area where within future sampling campaigns low-error burden samples could be collected.

2. Materials and Methods

2.1. Study Area

The Tisza River discharges the eastern part (area: 157,200 km²; length: 962 km) of the Carpathian Basin in Central Europe, while the Maros/Mures River is its most significant tributary (area: 30,000 km²; length: 750 km [50]). The study area extends 4.2 km downstream of the confluence of the Tisza and Maros Rivers (Figure 1).
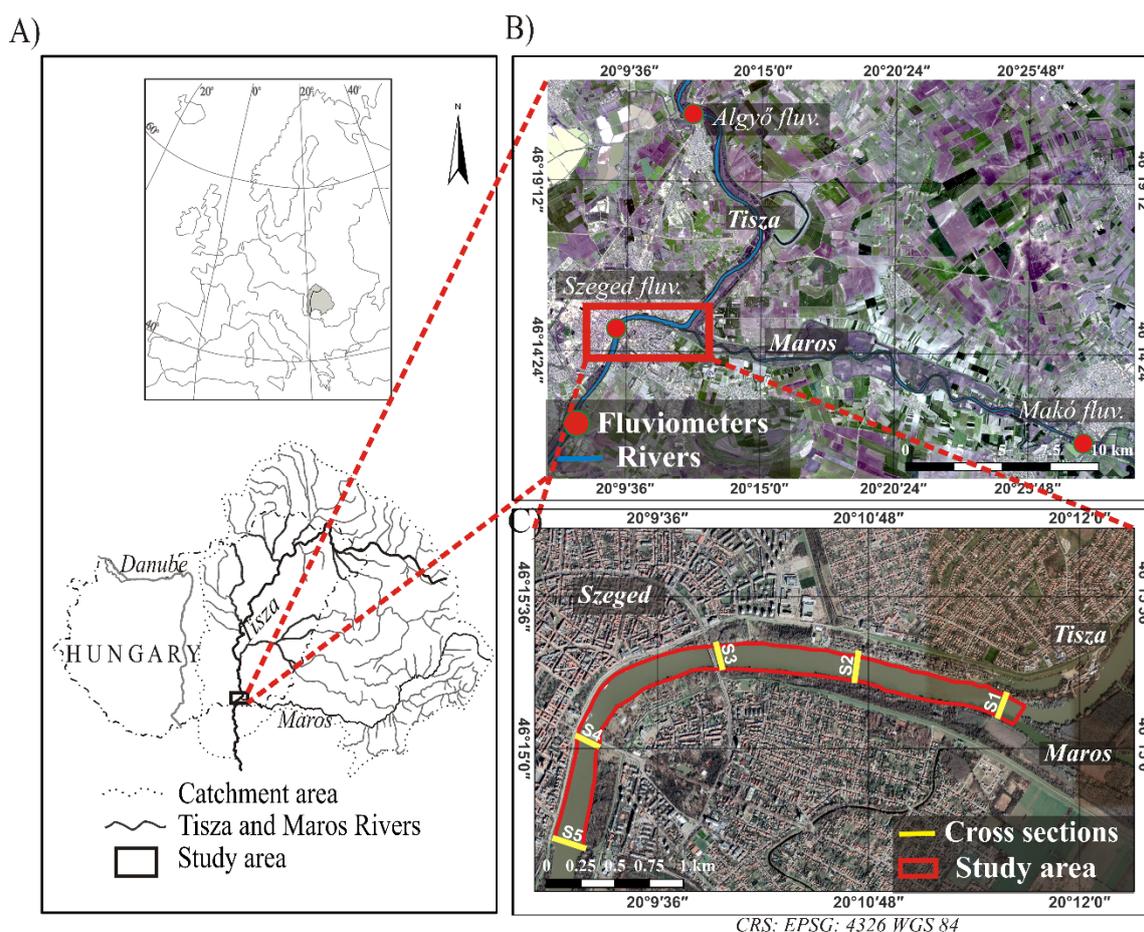
**Figure 1.** The confluence of the Tisza and Maros Rivers in Hungary was studied in detail. (**A**) Catchment area of the Tisza and Maros Rivers. (**B**) Locations of the three fluviometers along the Tisza (Algyő, Szeged) and Maros Rivers (Makó). (**C**) In the confluence area, the mixing was studied in detail at five cross sections (S1-5). (Source of the background images: B: Sentinel-2; C: Google satellite).

Both rivers have two floods within a year. The first and largest one occurs in early spring due to snowmelt, while the second flood occurs in early summer due to rainfall [51]. Floods usually inundate the floodplains of the Tisza River for 2–3 months, while they last only for 1–2 weeks on the Maros River. During simultaneous floods they can impound each other, or the Danube can impound them. As the Maros has a higher slope [50], it is impounded just along ca. 25 km long section (up to Makó gauging station). However, the Tisza with a lower slope [52] can be impounded by the Danube up to 330 km (to Szolnok). The Tisza enters the confluence area with a lower flow velocity (mean: 0.54 m/s) than the Maros (mean: 0.66 m/s).

The mean discharge of the Tisza is ca. sixfold of the Maros River (Table 1), though the difference between their maximum discharge is just 1.7 times [50]. The Maros transports three times more bedload, and it has ca. three times higher suspended sediment concentration than the Tisza River. The high sediment load of the Maros can be explained by the highly erodible rocks and steep slopes of its catchment, the steep valley and channel slope, and its rapid water level changes. However, as the result of greater water discharge, the annual suspended load of the Tisza is ca. twice as much as that of the Maros [53].

The confluence of the Maros is located at the 177 fluvial km of the Tisza River (0 fkm is at the confluence of the Tisza and Danube Rivers in Serbia). The confluence angle is 23°. The lower reach of the Tisza River is wider (bankfull width: 164 m) and deeper (bankfull depth: 14.1 m; recorded in 1999 [54]) than the lower reach of the Maros (width: 126 m; depth: 4.26 m; recorded in 1991 [53]). However, it should be noted that upstream of the confluence both rivers are much narrower (Tisza: 140 m; Maros: 70 m) and deeper (Tisza: 16.8 m; Maros: 4.8 m) as the result of intensive channel regulation works. The studied confluence zone extends 4.2 km downstream of the confluence point (Figure 1C). Here the channel is 170 m wide on average, and the mean thalweg depth is 13.6 m. However, in the confluence area, significant depth variations occur. The narrowest width (149 m) is associated with the greatest channel depth (18.6 m) at cross section No. S4. Meanwhile, the widest width (200 m) can be observed at S5, with a relatively shallow depth (11.6 m). The channel material is mainly clay.

Table 1. Main hydrological parameters of the Tisza at Szeged and the Maros River at Makó gauging stations. At the extreme values, the year of measurement is also indicated [50,55]).

		Tisza River	**Maros River**
Slope (cm/km)	Mean	2.4	28.0
Flow velocity (m/s)	Mean	0.54	0.66
Discharge (m³/s)	Maximum	4346 (1932)	2450 (1975)
	Mean	930	161
	Minimum	58 (2013)	21 (1919)
	Bankfull	2020	850
Water level (cm)	Maximum	1062 (2006)	615 (1975)
	Minimum	−293 (1968)	−113 (2012)
Transported sediment (t/y)	Suspended load	18.7 million	8.3 million
	Bed load	9000	28,000
Specific sediment load (t/m³)	Suspended load	6.4×10^{-4}	1.6×10^{-3}
	Bed load	3.1×10^{-7}	5.5×10^{-6}

The first channel regulation of the studied confluence dates back to the beginning of the 18th century when salt mining and logging flourished in Transylvania. As their main transport route was the Maros, its channel was cleared from shipping barriers [56]. Meantime, it was also a problem that the Maros joined the Tisza almost in the opposite direction (θ: 97°). Thus their floods blocked each other, creating extremely large floods, inundating the city of Szeged. In the 1830s there was a debate on the relocation of the conjunction

south of Szeged, but economically and commercially this would have adversely affected the city. According to the other plan, the location of the conjunction would have remained almost at the same place, but a new channel section of the Maros is created, so the confluence angle could have been reduced to ca. 23°. Finally, this plan was implemented in the mid-1850s [57]. However, the new conjunction was badly designed, thus during floods, the artificial channel section of the Maros was almost totally plugged by sediment, and the channel of the Tisza also became aggraded (depth: ≤1 m); thus, the intensive sand bar formation hindered shipping [56]. Therefore, additional plans were made to solve the problem. During the 1860s, the downstream section of the Maros was almost completely straightened, and stone bank protection was built [58], and the channel of the Tisza was narrowed by groynes.

2.2. Hydrological Data

Daily water stage (H) and discharge (Q) data were used for the period of January 2015–May 2021 from three gauging stations: the Makó gauging station is located on the Maros 24.5 km upstream of the confluence (Figure 1B), the Algyő fluviometer is located on the Tisza 14.9 km upstream of it, while the Szeged gauging station is located 3.4 km downstream of the confluence, approximately in the middle part of the study area. The water stage is measured by the local hydrological authority (ATIVIZIG) with a precision of ±0.5 cm. The daily discharge is calculated by the authority applying water level data. However, the discharge rating curves are recalculated monthly based on at-a-site measurements to ensure the quality of the collected data. Daily water level change (ΔH) was calculated at the three stations by subtracting the water level at a particular day from its counterpart on the previous day. The differences between daily water level changes between Tisza (Algyő) and Maros (Makó) were calculated by subtracting the daily change in Algyő ($\Delta H_{Algyő}$) from the daily change in Makó ($\Delta H_{Makó}$). The absolute difference in discharge (ΔQ) of the two rivers was calculated between Algyő and Makó, while their discharge ratio was calculated between Makó and Szeged stations ($Q_{Makó}/Q_{Szeged}$), which reflect the contribution of the tributary to the main river. In order to calculate the daily slope (S) of the water, the first step was to transform the relative stage data into absolute water levels (m asl.) based on the "0" points of the fluviometers (Makó: 79.50 m, Algyő: 74.00 m and Szeged: 73.70 m asl.). Then the length of the two rivers along their centerlines was measured between gauging stations. Finally, the daily water slope values represent the Tisza slope (S_{Tisza}) between Algyő and Szeged, and the Maros (S_{Maros}) between Makó and Szeged were calculated. To calculate the slope difference (ΔS) between the Tisza and the Maros Rivers, the daily slope data of the Tisza were extracted from the Maros data.

2.3. Remote Sensing Data

Between July 2015 and May 2021, altogether, 143 Sentinel-2 A-B satellite images (free of clouds to ensure the quality of the acquired data) covering the confluence area were downloaded from the Copernicus Open Access Hub [59]. Sentinel-2 captures the Earth with 13 spectral bands ranging from visible- to short-wave infrared [60]. The spatial resolution of the bands ranges between 10 to 60 m; the temporal resolution of the images is five days; however, it reaches three days at mid-latitudes such as the study area at Szeged [61]. The Sentinel-2 products take advantage of ground control points, which resulted in georeferencing accuracy of 12.5 m [62]. Furthermore, the mission's specifications set a limit of 5% radiometric uncertainty and a goal of 3% ideal accuracy [61], which is suitable for this application. The images taken in 2015 and 2016 were available only in level 1C; therefore, they were atmospherically corrected to remove the effects of atmosphere, which differs from time to time, guaranteeing the uniformity of the data and consequently its quality. Meanwhile, the rest of the images (2017–2021) were available in level 2A; thus, they were already atmospherically corrected. The Sen2Cor 2.8 processor, which is integrated with SNAP 8.0 software [59], was applied to perform the atmospheric correction process by converting the top of atmosphere reflectance into the bottom of atmosphere

reflectance in three steps (i.e., scene classification for cloud detection, deriving water vapor content and aerosol optical thickness, and finally, converting the top of atmosphere reflectance to the bottom of atmosphere reflectance [63]).

In order to mask the study area, the normalized difference water index (NDWI; developed by McFeeters and Stuart K [64]) was implemented on one image (9 April 2021) to extract water pixels only and to produce a shapefile for the confluence area. The NDWI depends on the reflectance of the near-infrared and visible green bands to enhance the presence of water. It was calculated by the "Band Math" tool in SNAP 8.0 software. Concerning the threshold value, it was identified by trial and error by comparing the output visually, as the authors performed several field campaigns in the study area; thus, they could distinguish the water and non-water pixels. The produced shapefile was used to mask the confluence area on all 143 images.

The high contrast of the reflectance of pixels between the water of the two rivers in the confluence area, which resulted from the difference in their suspended sediment load, was exploited to study the mixing process in the confluence using an unsupervised classification technique. The K-means unsupervised classification algorithm [65] was applied to classify pixels based on their reflectance value to discriminate between the surficial suspended sediment concentrations of both rivers in the confluence area. The general theory of this algorithm is to identify a centroid for every cluster (k), then every point in the data is allocated to each cluster by reducing the sum of the square error to the centroid [65,66]. The number of clusters is identified by the user according to the nature of the data. The algorithm begins the learning process by identifying random centroids; afterwards, it performs repetitive iterations to optimize their positions. The optimization process halts when the centroids stabilize, or when the maximum number of iterations is achieved [65]. In the present study the bands 2, 3 and 4 of Sentinel-2 were chosen for classification, due to their relatively high spatial resolution (10 m), and their sensitivity to suspended sediment concentration [67–70].

The pixels were classified into three classes, representing the water of the Tisza (TW), which usually has lower suspended sediment concentration; the water of the Maros (MW) with higher suspended sediment concentration; and their mixture (MIX), which has a moderate amount of suspended sediment. The threshold of reflectance of MW in bands 2, 3 and 4 are 0.057, 0.084 and 0.081, respectively, while in the case of MIX, it is 0.055, 0.078, and 0.063, and for TW, it is 0.052, 0.072, and 0.050, respectively. It also demonstrates the reflectance gradient from the lowest values in case of TW to the highest in case of MW. However, these threshold values are an example of one image acquired on 9 April 2021, as they could change temporally because of (1) the dynamism of suspended sediment load transported by the studied rivers, and (2) the changes in chemical and biological processes which affect the water quality of both rivers, and consequently the spectral reflectance of the water surface. Therefore, K-means was applied to accommodate the threshold dynamism, as it automatically selects the threshold of the three bands based on reducing the sum of square error of pixels to the centroid of each class. Despite the algorithm's automated process, every image was analyzed individually to make sure that the actual mixing situation was represented perfectly. In order to avoid misclassification problems which would arise from defining three classes only (due to the existence of shadow developed by trees or bridges), more than three classes were defined, then they were merged to form the TW, MW, and MIX classes. The number of classes was identified by trial and error, comparing the results with the visual overview of the confluence to achieve the most representative classification of the mixing process. The area of the shadow class was extracted from the whole study area. Then the area occupied by the three water types was recalculated and expressed as the proportion of the study area (%).

The areal distribution (%) of the water classes (TW, MIX, and MW) was calculated on all 143 images. The longitudinal mixing was studied by measuring the longitudinal extent (L) of the water of the Maros (MW) into the Tisza as a function of the average width (w) of the Tisza River in the study area (162.2 m). The lateral mixing was also evaluated along

five cross sections (S1–5) spaced 1 km apart (ca. 6-times of the width of the Tisza; Figure 1C). Along these cross sections the width of MW, MIX, and TW were measured and divided by the cross-section width to convert it to a percentage, which demonstrates the dominancy of each water type along a cross section.

2.4. Correlation between Hydrology and Suspended Sediment Dynamism: Statistical Analysis

The correlation between all measured and calculated hydrological parameters at the three gauging stations (Algyő, Szeged, and Makó) and the spatial and temporal characteristics of the mixing waters (TW, MW, and MIX) were analyzed based on the Pearson correlation matrix. The correlation coefficient (r) was interpreted as very weak $0.0 \leq r \leq 0.19$, weak: $0.2 \leq r \leq 0.39$, moderate: $0.4 \leq r \leq 0.59$, strong: $0.6 \leq r \leq 0.79$ and very strong: $0.8 \leq r \leq 1.0$ [71]. Hierarchical cluster analysis (HCA) was applied to classify the images into two groups based on the calculated area (%) of various waters (TW, MW, and MIX) and the hydrological parameters. In this study, Ward's algorithm [72] was used to classify the data, defining the similarity between the clusters based on the summation of squares within the clusters aggregated overall object. Finally, the stepwise multilinear regression technique was applied to produce predictive equations for the areal percentages of various waters (TW, MW, and MIX) in the confluence area and the longitudinal extent of the Maros into the Tisza (L), considering the various hydrological parameters as independent variables. The predictive equations were produced for three cases of data. In Case 1, all data were considered; thus, the resulted equations can be used at any discharge or water stage, and they produce rough predictions, as these models were built based on all measured and calculated data. In Case 2, the data of cluster I were considered, thus the model can be used for predictions with low or medium discharges, while in Case 3, only the cluster II data were dealt with; thus, it is suitable to predict the mixing conditions during high (flood) discharges. All the applied statistical analyses were performed by IBM SPSS software v26.0 [73].

3. Results

3.1. Hydrological Characteristics of the Studied Period

No considerable flood appeared on the studied rivers during the studied period. Five small overbank floods (Algyő: ≥610 cm; Szeged: ≥500 cm) were recorded in the Tisza River at Szeged (Figure 2), whereas just two floods developed on the Maros (Makó: ≥310 cm). These floods created shallow inundations on the floodplains (at Szeged: 6–30 cm; at Algyő: 59–98 cm; at Makó: 18–65 cm). On both rivers, floods developed from February to July; only one of their flood waves coincided (June 2020). The near bankfull stages (at and below bankfull stage by 1.0 m) were more common on both rivers, and they were recorded in the same late winter and spring months. During floods or near-bankfull levels, the Tisza usually had a flood peak simultaneously or slightly later (by 1–2 days) than the Maros (Figures 2 and 3).
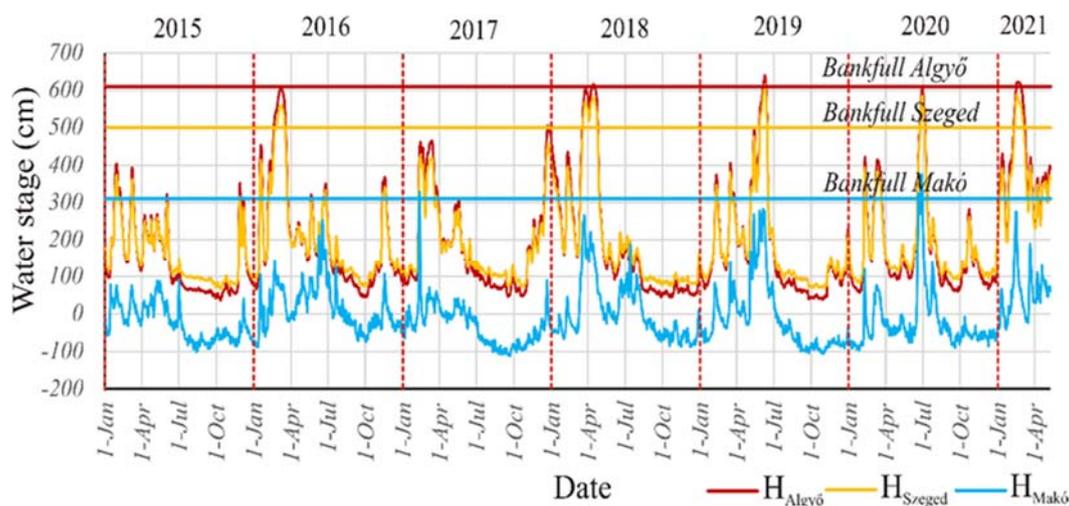
Figure 2. Daily water stages and bankfull levels at the studied gauging stations of the Tisza (Algyő and Szeged) and Maros Rivers (Makó) throughout the studied period (January 2015-May 2021).
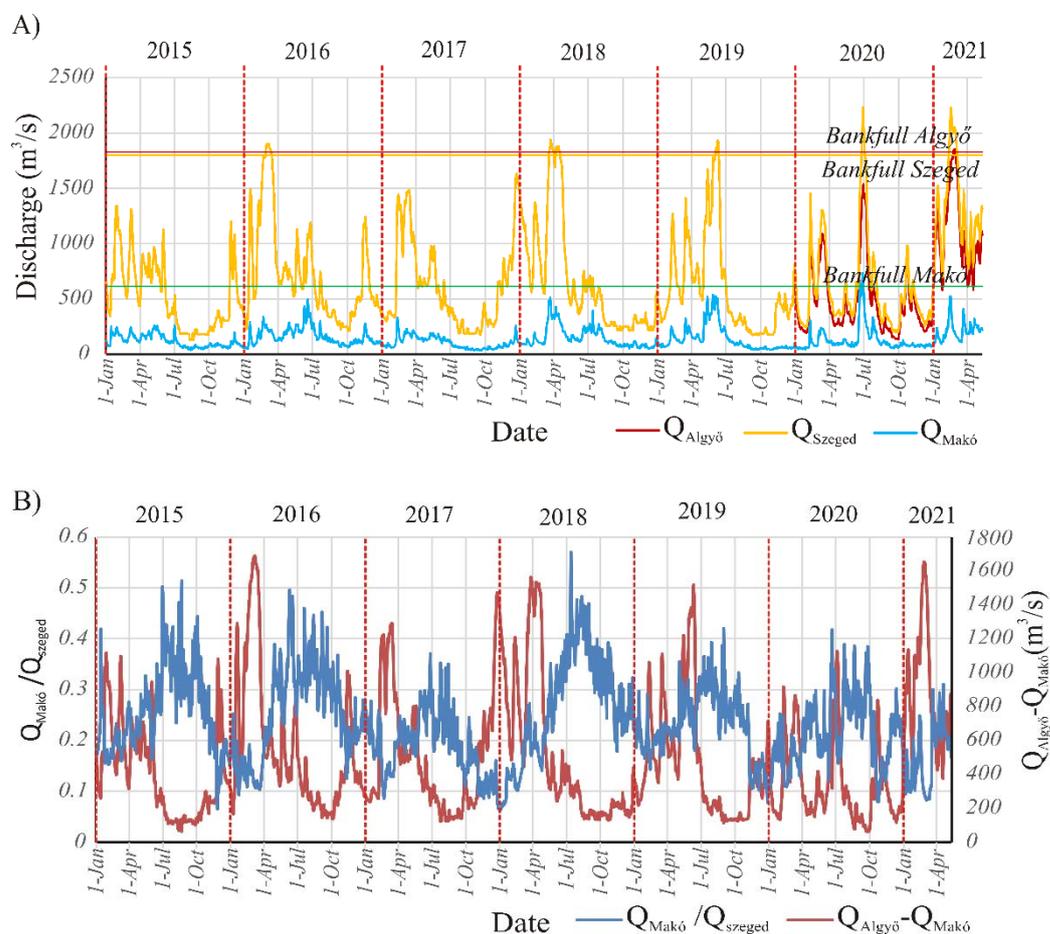
Figure 3. (**A**) Daily discharge values at the three gauging stations and (**B**) the discharge ratio ($Q_{Makó}/Q_{Szeged}$) and difference ($Q_{Algyő}$-$Q_{Makó}$) at the gauging stations of the Tisza (Algyő and Szeged) and the Maros (Makó) in the studied period (January 2015–May 2021).

Low stages were recorded in the Tisza River, usually between August and January. Similar to floods, the low stages developed on the Tisza simultaneously or slightly later (by 1–4 days) than on the Maros. The lowest water stages in both rivers (Algyő < 60 cm; Makó < −100 cm) were usually measured between August and November. During the studied period, low stages were the dominant stages in both rivers, as their probabilities

were nearly 80%, and the mean and mode values of annual stages shifted towards low waters (Figures 2 and 3).

In the confluence zone, the mixing of the water of the two rivers might be influenced by the daily stage changes of the two rivers; therefore, it was calculated and analyzed (see Appendix A, Figure A1). Furthermore, the absolute difference in daily water level changes between Algyő and Makó was also calculated (Figure A1). The data reflect that the Maros had more significant variations in water stages during floods than the Tisza.

In the studied period, during floods, the discharge in the Tisza River varied between 827 and 2087 m³/s (Table 2), while the Maros had only 70–731 m³/s discharge. In non-flood periods the Tisza had 128–1045 m³/s discharge, while the Maros had just 30–393 m³/s. However, the ratio between discharges is more informative (Figure 3). The ratio between the discharge measured at Makó and Szeged refers to the contribution of the Maros to the discharge of the Tisza downstream of the confluence (at Szeged). It can be observed that the highest numbers (greater contribution of the Maros) appeared during low stages in both rivers, usually in the winter months or during summer or early autumn. In these cases, the discharge ratio was 0.37–0.57; thus, the Maros contributed by 37–57% to the discharge of the Tisza. The lowest discharge ratios (0.06–0.10) were recorded usually in the winter months, when the Maros increased the amount of transported water of the Tisza just by less than 10%.

Table 2. Descriptive statistics of the measured and calculated hydrological parameters at the three studied fluviometers.

	Station	Range	Min.	Max.	Mean	Std. Dev.	Median	Mode
Water stage (cm)	$H_{Algyő}$	604	36	640	190	144	140	64
	H_{Szeged}	549	66	615	195	123	149	94 [1]
	$H_{Makó}$	487	−112	375	−7	74	−24	−77
Absolute water level (m)	abs. $H_{Algyő}$	6.04	74.36	80.40	75.91	1.44	75.40	74.64
	abs. H_{Szeged}	5.49	74.36	79.85	75.65	1.23	75.2	74.64 [1]
	abs. $H_{Makó}$	4.87	78.38	83.25	79.43	.74	79.26	78.73
Slope (cm/km)	S_{Tisza}	5.5	0.0	5.5	1.4	1.2	1.1	0.0
	S_{Maros}	16.9	2.7	19.6	13.0	2.8	13.9	14.3
	S_{Tisza}−S_{Maros}	20.8	−18.8	2.0	−11.6	3.9	−13.1	−14.4 [1]
Discharge (m³/s)	$Q_{Algyő}$	181,200	128	1940	627	425	501	180 [1]
	Q_{Szeged}	210,500	128	2233	659	448	520	180 [1]
	$Q_{Makó}$	701	30	731	137	91	110	75
	$Q_{Algyő}$−$Q_{Makó}$	1629	60	1689	490.5	363.5	376.5	139
	$Q_{Makó}$/Q_{Szeged}	0.51	0.06	0.57	0.23	0.09	0.22	0.20

[1] Multiple mode exist. The smallest value is shown.

In the studied period, usually, the Maros had a ninefold greater slope than the Tisza (Table 2, Figure 4). The Maros had greater variations in slope, as it had a range of 16.9 cm/km (min: 2.7 cm/km; max: 19.6 cm/km), while it was only 5.5 cm/km for the Tisza, respectively (min: 0.0 cm/km; max: 5.5 cm/km). Usually, during floods, the slope of the Tisza ranged between 1.3 and 5.5 cm/km, while the Maros had a 2.7–19 cm/km gradient. However, during non-flood periods the slope of the Tisza dropped considerably (0.0–3.4 cm/km), whereas the Maros kept the high slope values (8.4–19.6 cm/km). The temporal change of slope conditions of the Tisza River opposes its counterpart of the Maros River (Figure 4), thus when the slope of the Tisza increased (following the same pattern as the stage and discharge), usually the slope of the Maros decreased, referring to impoundment.
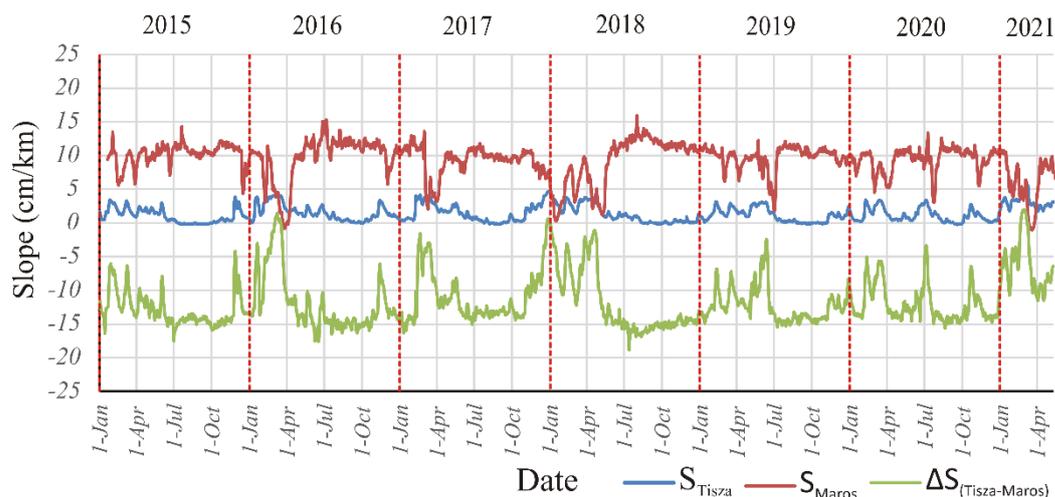
Figure 4. The calculated daily slope of the Tisza and Maros Rivers and their slope difference (ΔS) throughout the studied period (January 2015-May 2021).

The difference in slope conditions was also analyzed, as it can fundamentally influence the mixing of the waters of the two rivers. The slope differences between the Tisza and Maros showed significant temporal variations, as the difference could be as high as 20.8 cm/km (min: −18.8 cm/km, max: 2 cm/km). The Tisza and the Maros had very similar slope conditions; only when the slope of the Maros declined (due to impoundment), and the Tisza had a high slope during a flood wave, the difference between their slope values get close to 0 cm/km or above it. Such cases were observed in late winter and early summer. On the contrary, the negative values (<−17 cm/km) refer to the high slope on the Maros due to its small flood wave and a simultaneous low stage of the Tisza, when the Törökbecse Lock impounded it. This situation was observed in the summer months (June–July), when the Maros had a greater slope than the Tisza by 17.4–18.2 cm/km.

3.2. Mixing of Waters in the Confluence Area—General Characteristics

In the study area, the Tisza (TW) and Maros waters (MW) and their mixing (MIX) showed characteristic spatio-temporal variations throughout the studied period (Figure 5). Usually, the water of the Tisza dominated the confluence area (mean areal proportion: 48.7%), while the Maros water occupied a much smaller area (mean: 12.4%), but their mixed water also occupied high proportions (mean: 38.9%). When there was a flood on the Tisza, the incoming Tisza water was even more dominant, as it occupied 60–100% of the confluence area. In some cases, the Maros water covered as much as 10–25; however, during a flood (June 2020), it covered 55.5% of the confluence due to its high water level. On the other hand, the mixed water of both rivers changed within a wide range (0–52%).
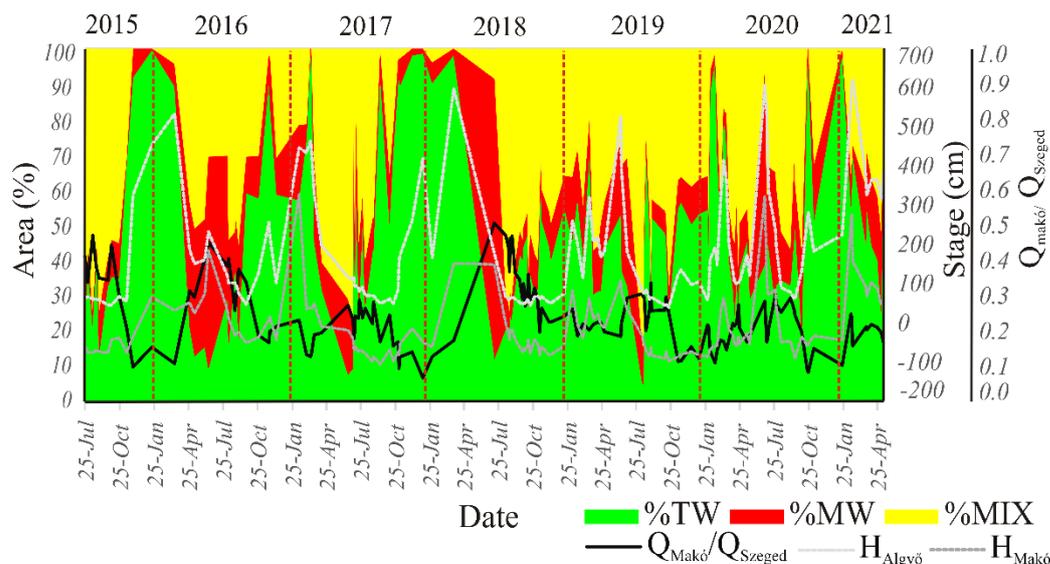
Figure 5. Areal distribution (%) of Tisza water (TW), Maros water (MW), and their mixed water (MIX) in the entire confluence area based on the acquisition of 143 Sentinel-2 images. The main characteristics of the concurrent rivers are also indicated.

The areal changes of the water of the Tisza (TW) compared to the variations of hydrological parameters can help to understand the mixing process. For instance, during simultaneous bankfull or over bankfull (flood) events (e.g., January 2016, December 2017, and March 2018), the dominancy of TW was found in the confluence area, as the Tisza water covered 98–99.5% of the area.

On the other hand, in the confluence zone, the Maros water (MW) had more complex temporal changes (Figure 5), as it had minimal coverage when the Tisza had bankfull/over bankfull stages and also during simultaneous low stages. However, the highest coverage of the Maros was achieved when both rivers had near-bankfull stages. Thus, the high stage of the Maros resulted in elevated momentum values, which enabled the river to interact more with the Tisza. Therefore, the MW seemed to negatively correlate with the stages greater than bankfull level in both rivers; however, it had a positive correlation with the stages below that level.

The proportion of mixed waters of the two rivers (MIX) was in closer correlation to the areal percentage of TW than to the MW (Figure 5). The highest MIX percentages were observed during low stages in both rivers, whereas the lowest mixing occurred during flood periods in both rivers.

The spatial distribution of the three water types was studied along cross sections (S1–S5), to reveal characteristic patterns (Figure 6).
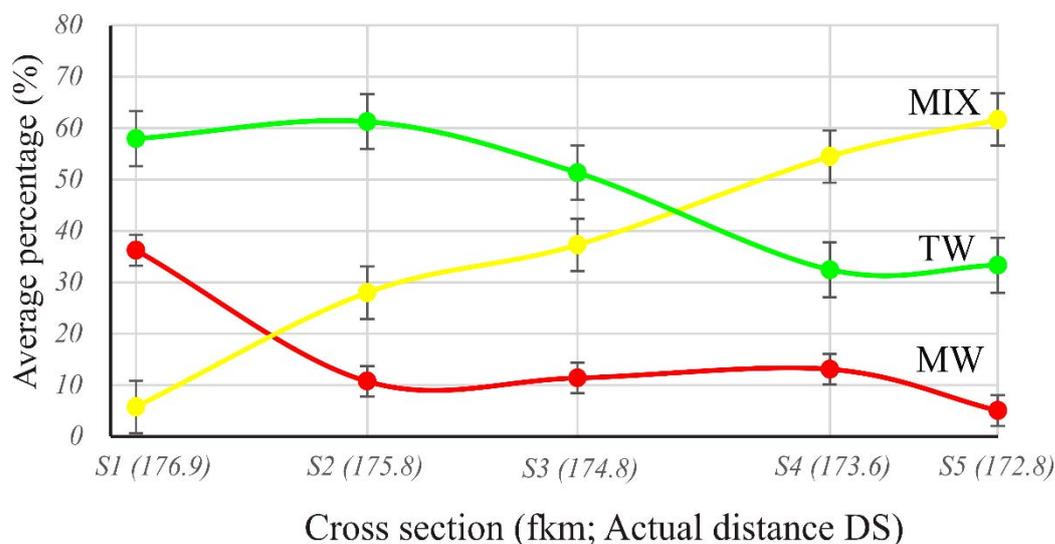
Figure 6. The mean percentage of the Tisza water (TW), Maros water (MW) and their mix (MIX) along five cross sections downstream of the confluence point based on the acquisition of 143 sentienl-2 images. The error bars indicate a 95% confidence interval.

In general, the TW and MW had a decreasing trend from S1 towards S5, while the mixed water increased. The TW proportion slightly increased between S1 and S2 (from 58% to 61%), then it dropped gradually until S4 (32%), and finally, it was almost stabilized between S4 and S5. However, during floods, the TW had almost full lateral coverage along all cross sections (see the heat map in the Appendix A, Figure A2). On the contrary, the proportion of the MW decreased suddenly between S1 (36%) and S2 (11%), and then it remained the same; however, it decreased substantially again by the last cross section (S5: 5%). However, when the Maros had near bankfull level, and the water stages in the Tisza were relatively low, the MW was represented in all cross sections with an average lateral percentage of 35% (Appendix A Figure A2). The gradual areal decrease of the waters of the two rivers and the simultaneous increase of the mixed water reflected the gradual mixing of the waters towards downstream. The MIX water usually did not have any coverage at the first cross section as the joining waters just interacted (Appendix A Figure A2), furthermore, it was only slightly represented during floods, as the study area was already covered by the Tisza or the Maros water. However, the MIX had significant coverage during low stages in both rivers (summer and autumn) when it appeared between the S2 and S5 cross sections.

The distance (L) of the last downstream Maros water pixel was measured from the conjunction point to reveal the longitudinal dimension of the mixing (Figure 7). The longitudinal extent of MW into the Tisza River was 1.3 km on average, thus 7.8 times of the Tisza's channel width (w). However, it had significant variations throughout the studied period, as it varied from 650 m to kilometers (4–26 w). It can be noticed that the temporal changes of the longitudinal extent of MW corresponded to the temporal pattern of the areal percentage of MW; thus, it reached its peaks at near bankfull stages mostly at summer times and had the shortest extent during late summer or autumn low stages, or at near bankfull stages in late winter or early spring.
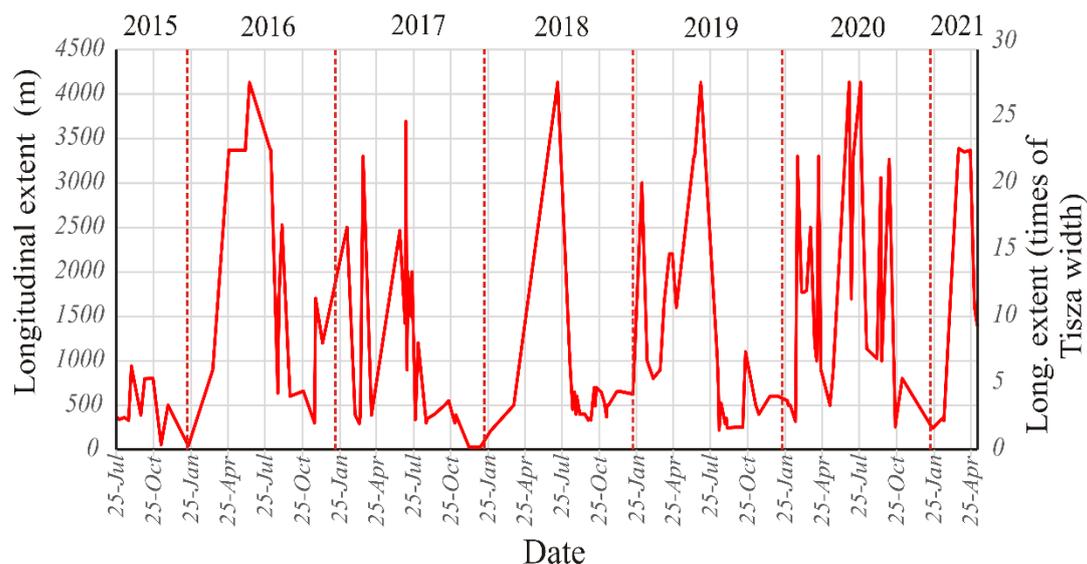
Figure 7. The longitudinal extent of Maros water (MW) into the Tisza River in the studied period.

3.3. Hydrological Parameters and Mixing

The relationship between TW, MW, and MIX and the various hydrological parameters of the joining rivers were analyzed in detail, as probably the dominance of one or another water reflects the weight of rivers from the point of view of their hydrological parameters (see Appendix A, Figure A3). The discharge ratio was in the closest relationship to water types (especially TW and MIX) at any water stage; however, the slope and discharge differences between the rivers showed a weaker correlation with the area of waters with various origins. However, the slope and discharge differences between both rivers suggest that it must be considered whether it was a period with low slope during low stages or impoundment, or a high slope period during flood waves. This was also confirmed by the HCA analyses as it classified the data into two clusters. Those mixing patterns belonged to Cluster I, which developed at low and medium discharges ($Q_{Tisza} \leq$ 747 m³/s and $Q_{Maros} \leq$ 150 m³/s), while Cluster II contained mixing patterns developing at high discharges.

To support these statements, a correlation matrix was created between (1) the areal percentage of waters (TW, MW, and MIX) and the longitudinal extent of MW in the confluence area, and (2) the various measured and calculated hydrological parameters (Table 3). Based on the Pearson correlation matrix, there was a moderate to strong correlation between the areal percentages of water pixels (TW, MW, and MIX) and water level, slope, slope difference, discharge, discharge ratio, and discharge difference; and very weak correlation with the daily change of water level (ΔH) and the difference between the two river's daily stage changes. The areal distribution of the main river's water (TW) showed a strong positive correlation with ΔS (r: 0.65), and a strong negative correlation with $Q_{Makó}/Q_{Szeged}$ (r: −0.73) and S_{Maros} (2: −0.65). The MIX water showed relatively similar correlations as the TW, as it showed a strong positive correlation with $Q_{Makó}/Q_{Szeged}$ (r: 0.67), and S_{Maros} (r: 0.6), and strong negative correlation with S_{Tisza} (r: −0.66), ΔS (r: −0.64) and ΔQ (r: −0.63). The areal extent of the tributary (MW) showed less sensitivity to the hydrological parameters than TW and MIX. It showed the best correlation with the hydrological parameters measured at Makó gauging station, as it showed a moderate positive correlation with $Q_{Makó}$ (r: 0.5), $H_{Makó}$ (r: 0.47), $Q_{Makó}/Q_{Szeged}$ (r: 0.31), and S_{Maros} (r: 0.27).

Table 3. Pearson correlation matrix between the areal distribution (%) of mixing waters (TW, MW and, MIX), longitudinal extent (L) of Maros water (MW) in the confluence area, and the various hydrological parameters.

	TW	MW	MIX	L
TW	1.00			
MW	−0.46	1.00		
MIX	−0.91	0.04	1.00	
$H_{Algyő}$	0.43	0.12	−0.54	
H_{Szeged}	0.40	0.13	−0.51	
$H_{Makó}$	0.02	0.47	−0.24	
S_{Tisza}	0.57	0.03	−0.66	
S_{Maros}	−0.65	0.27	0.60	
ΔS	0.65	−0.18	−0.64	
$\Delta H_{Algyő}$	0.01	−0.10	0.03	
ΔH_{Szeged}	0.01	−0.10	0.04	
$\Delta H_{Makó}$	−0.12	0.07	0.10	
$\Delta H_{Algyő}$-$\Delta H_{Makó}$	0.11	−0.15	−0.05	
$Q_{Algyő}$	0.48	0.10	−0.58	
Q_{Szeged}	0.42	0.13	−0.54	
$Q_{Makó}$	0.01	0.50	−0.24	
$Q_{Makó}/Q_{Szeged}$	−0.73	0.31	0.67	
ΔQ	0.57	−0.02	−0.63	
L	−0.36	0.85	−0.01	1.00

The longitudinal extent of MW into the Tisza showed very similar correlations to the areal percentage of MW, as it had the highest correlation with $H_{Makó}$ and $Q_{Makó}$ (r = 0.5 and 0.5 respectively). Thus, the TW and MIX showed their highest correlations with discharge ratio between the two rivers, slope and their slope difference, while the MW showed less sensitivity to discharge ratio and water slopes, and higher sensitivity to discharge and water level measured at Makó gauging station. Thus, it can be concluded that the areal distribution of TW and MIX waters in the confluence area were highly correlated to each other and most of the hydrological parameters of both rivers, whereas the areal distribution of MW was mainly dependent just on the hydrology of the Maros.

In order to understand the mixing processes, some events were selected, when the Tisza and the Maros had very different (low versus high stage) or very similar hydrological situations (i.e., both rivers had floods or low stages). During the studied period, simultaneous floods on both rivers occurred just once, on 30 June 2020, when both rivers reached a peak, the Tisza stage was 585 cm (Szeged) and Maros had 324 cm (Makó). It must be noted that it was a very small flood, as the recorded highest flood was ca. 500 cm higher at both gauging stations. During this event, the mixing was very limited, as the TW and MW had high areal coverage (TW: 38.8%, MW: 55.6%), while the MIX had a very low area (5.6%). The lowest stages in both rivers were recorded on 19 October 2019 (the Tisza at Szeged: 72 cm; Maros at Makó: −96 cm). In this hydrological situation, the MIX dominated the confluence area (67.7%), while the TW and MW areas were limited (24.2% and 8.0%, respectively). In this hydrological situation, the Tisza appeared (upwelled) at the downstream half of the confluence area (S3–S5). Those hydrological situations when the water stages in both rivers were in an adverse condition (high vs. low) were analyzed as well: on March 18th 2016, the greatest difference between the water stages (Tisza (Szeged): 491 cm; Maros (Makó: 33 cm) occurred throughout the studied period. On this day, the Tisza covered almost the whole study area (TW: 89.3%, MW: 6.4%, and MIX 4.4%) without any upwelling, and the water of the Maros was detected along the first three sections (S1–3). In an adverse situation, on 14 July 2018, the Maros had a relatively high stage (Makó:

150 cm), and the Tisza had a low stage (Szeged: 193 cm). At this time, the MW was dominant in the confluence zone (TW: 12.1%, MW: 79.3%, and MIX: 8.5%), and no upwelling occurred.

3.4. Main Patterns of Mixing Waters

The previously illustrated spatio-temporal changes of the mixing waters in the confluence area had characteristic patterns. Considering the areal dominancy of each water type, three main mixing patterns were identified: TW dominant, MW dominant, and MIX dominant (Table 4, Figure 8). Within the TW and MIX classes, further subclasses were identified considering the spatiality of the mixing, and the appearance of one of the waters at the end of the study area ("upwelling pattern"). Within the MW dominant class, no upwelling from any other waters was observed, so this class has no subclasses.
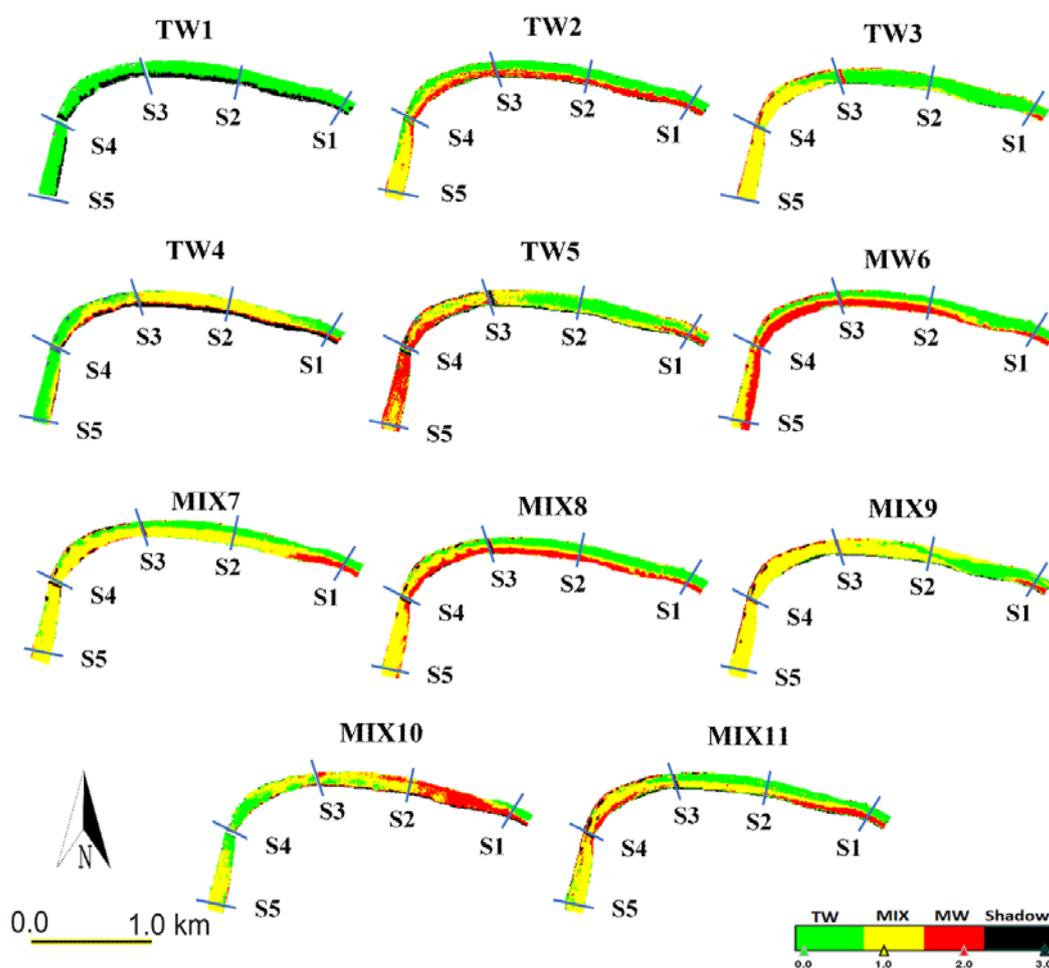
Figure 8. Examples of the eleven identified mixing patterns.

In the patterns of the first class, the TW dominated most of the confluence area (Table 4, Figure 8). Sometimes, at the end of the study area, the sudden appearance (upwelling) of one of the rivers was visible (TW4 pattern: Tisza; TW5 pattern: Maros). In other cases, the upwelling was not obvious (TW1–TW3).

Table 4. Main characteristics of the identified mixing patterns.

Mixing Type (Class)	Up-Well-ing	Sub-Class	Characteristics of Water Types [1]			Characteristic Hydrological Parameters				Frequency (%)	Appearance (Months) [2]
			TW	*MW*	*MIX*	$Q_{Makó}/Q_{Szeged}$	$Q_{Algyő}-Q_{Makó}$ (m³/s)	$\Delta H_{Algyő}-\Delta H_{Makó}$ (cm)	$\Delta S_{(Tisza-Maros)}$ (cm/km)		
TW dominant	No	TW1	S1–S5: 70–100%	S1: 0–30%	no	0.1–0.34	151–1290	−27–54	−15.5–−1.4	18.9	**I-III**, IX-XI-XII
		TW2	S1–S4: 30–75%	S1–S4: 37–46%	S1–S5: 5–100%	0.11–0.26	142–1454	−56–56	−13.9–−0.3	17.5	I-III, VIII
		TW3	S1–S3: 30–100%	S1: 20–30%	S3–S5: 70–100%	0.17–0.26	142–1537	−11–22	−14.4–−2.3	4.9	III, IX-XII
	Tisza	TW4	S1 and S3–S5: 60–100%	S1–S4: 5–35%	S1–S5: 10–100%	0.11–0.29	102–597	−14–21	−14.7–−11.1	5.6	II, IX-XI
	Maros	TW5	S1–S3: 55–95%	S1 and S3–S5: 20–95%	S1–S5: 10–80%	0.15–0.25	103–511	−7–22	−13.8–−11	2.1	V, IX, XI
MW dominant	No	MW6	S1–S4: 10–75%	S1–S5: 30–80%	S1–S5: 10–60%	0.28–0.51	292–840	−42–35	−17.7–−8.2	4.9	IV, **VI-VIII**
MIX dominant	No	MIX7	S1–S4: 10–60%	S1–S2: 5–85%	S1–S5: 5–100%	0.2–0.41	108–617	−15–14	−15.5–−8.7	6.3	II, IV, V, VII-**VIII-X**
		MIX8	S1–S4: 10–70%	S1–S4: 30–40%	S1–S5: 5–100%	0.17–0.41	185–1104	−22–13	−15.7–−3.4	9.8	IV, VII-VIII, X
		MIX9	S1–S3: 5–95%	S1: 5–30%	S1–S5: 5–100%	0.2–0.5	68–544	−25–25	−16.6–−11.1	16.1	IV, VII-**VIII-IX**, **XI**
	Tisza	MIX10	S1 and S2–S4: 65–100%	S1–S2: 35–100%	S2–S3 and S4–S5: 10–100%	0.17–0.34	122–417	−16–11	−14.8–−11.6	12.6	III-IV, VII-VIII, X, XII
	Maros	MIX11	S1–S3: 45–65%	S1–S2 and S3–S4: 15–35%	S1–S5: 5–100%	0.22–0.3	265–548	−9–7	−14.5–−11.6	1.4	IV, VIII

[1] S1–S5: Those cross sections are indicated where the given water type appears. The % refers to the lateral contribution of the water type within these cross sections. [2] Those months are highlighted by bold fonts when the given pattern appears frequently.

In the case of TW1, minor mixing could be observed (Table 4, Figure 8): the TW dominated the confluence area (S1–S5: 70–100%), with a very limited extent of MW (just at S1: 0–30%) and no real mixing of the two water types. This pattern appeared in the winter months, usually in January and November when the discharge of the tributary was very low compared to the Tisza (mean $Q_{Makó}/Q_{Szeged}$: 0.16; mean ΔQ: 618 m³/s), the stage of the Tisza fluctuated more (mean $\Delta H_{Algyő}-\Delta H_{Makó}$: 1.9 cm), and it had a slightly higher slope; thus, the slope difference of the two rivers was less characteristic (mean ΔS: −9.6 cm/km). This pattern had the highest occurrence frequency (18.9%).

In the subsequent subclasses (TW2 and TW3), considerable mixing was apparent (Table 4, Figure 8); the difference between them was the appearance of MW. In the TW2 subclass, the MW was identified along most of the confluence zone (S1–4), and the MIX was characteristic at all cross sections. This pattern was characteristic in February and March when the Maros had increased discharge compared to TW1 (mean $Q_{Makó}/Q_{Szeged}$: 0.19; mean ΔQ: 788 m³/s), and the Maros had greater changes in stage (mean $\Delta H_{Algyő}-\Delta H_{Makó}$: −5.6 cm), but the slope changes were similar to the TW1 pattern (mean ΔS: −8.2 cm/km).

In the case of TW3, the MW appeared just at the beginning of the confluence zone (S1), while the MIX appeared in the second half (S3–5) of the confluence zone (Table 4, Figure 8), but its extent could reach 100% at particular sections. This subclass appeared in December when the difference between the discharge of the two rivers was smaller than in case of the TW1 or TW2 (mean $Q_{Makó}/Q_{Szeged}$: mean: 0.22; mean ΔQ: 476 m³/s); however, a tiny flood wave appeared on the Tisza (mean $\Delta H_{Algyő}-\Delta H_{Makó}$: 3.9 cm), though the slope of the Maros was still higher (mean ΔS: −11.6 cm/km).

The upwelling of the Tisza was observed in case of the dominancy of TW (Table 4, Figure 8). The characteristic feature of the TW4 pattern was the disappearance of TW at the confluence area (within S1) and afterwards it reappeared at the downstream of the confluence (between S3 and S5), as the TW seemed to be blocked by the MIX due to the stratification of MIX water above the TW. Though the MIX extended between S1 and S5 and had high lateral coverage, which could reach to 100% at some cross sections, the TW had the greatest areal percentage; therefore, the TW4 pattern was grouped into TW dominant condition. On the other hand, the MW could be identified along the study area too, but with limited lateral extent (5–35%). The TW4 usually appeared in October and November, when both rivers had low stages, and the discharge difference between the Tisza and Maros decreased (mean ΔQ: 323 m³/s), and the slope of the Maros increased (mean ΔS: −12.9 cm/km). However, the discharge ratio and the daily water change difference did not change significantly (mean $Q_{Makó}/Q_{Szeged}$: 0.2; mean $\Delta H_{Algyő}–\Delta H_{Makó}$: −4.4 cm).

In the case of the TW5 pattern, the upwelling of the Maros was observed during the dominancy of TW (Figure 8). The characteristic feature of the TW5 pattern was the disappearance of MW at the confluence area (within S1) and its reappearance between S3 and S5 cross sections. It seemed that the lower density TW stratified above the MW, probably because the TW had lower suspended sediment concentration. In this pattern, the TW was dominant (55–95%) but just at the upstream half of the study area (S1–S3), and at the downstream half, the MW had great lateral extent (up to 95%). The MIX appeared in all cross sections, but with limited lateral extent (10–80%; mean: 25%). Due to the low occurrence probability of this pattern (2.1%), it did not have a characteristic occurrence period; however, it had very similar hydrological parameters to the TW4 pattern (mean $Q_{Makó}/Q_{Szeged}$: 0.2; mean ΔQ: 363 m³/; mean $\Delta H_{Algyő}–\Delta H_{Makó}$: 4.7 cm; mean ΔS: −12.1 cm/km).

The pattern MW6 represented the case when the MW was dominant in the entire confluence zone (Table 4, Figure 8), covering a wide area (30–80%). The TW was also identifiable (S1–S4: 10–75%), as well as the MIX (S1–S5: 10–60%); however, their lateral coverage was smaller than, for example, in subclass TW2. The MW6 pattern usually appeared in June and July when the discharge of the Maros was high compared to the Tisza (mean $Q_{Makó}/Q_{Szeged}$: 0.34; mean ΔQ: 454 m³/s) and when they had a low slope difference (mean ΔS: −13.7 cm/km). This pattern had no further subclasses, and its occurrence frequency was 4.9%.

Concerning the MIX dominant class, five subclasses were identified, similarly to the TW class (Table 4, Figure 8). In the case of MIX7–MIX9 subclasses, the mixed water appeared at every cross section (S1–S5), and the contribution of the mixed water was 5–100%; additionally, none of the waters reappeared (no upwelling) at the downstream end of the confluence area. The specialty of the MIX7 subclass was that the MIX appeared in the entire study area (S1–S5). Nevertheless, TW was detectable along most of the confluence zone (S1–S4: 10–60%), but the MW appeared just on a short section (S1–S2) in a wide strip (5–85%). This mixing pattern usually appeared in August and October.

The MIX8 mixing pattern was similar to MIX7; however, the MW in MIX8 had a longer appearance (S1–S4), though with a narrower lateral extent (30–40%). Although the MW had a significant coverage in MIX8, which was similar to TW2 and MW6 patterns, the MIX had the largest percentage; therefore, it was grouped into the "MIX dominant" condition. This pattern was typical in the summer months (July and August).

In the subclass MIX9, the MW has the lowest contribution, as it appeared just at the beginning of the study area (S1), and here, its width was only 5–30% of the section. Meanwhile, the TW had a shorter longitudinal extent (S1–3) than in subclasses MIX7 and MIX8, though its proportion was higher (5–95%). On the other hand, the MIX also showed very high coverage (S1–5; 5–100%), similarly to the MIX7 and MIX8 patterns. The MIX9 mixing pattern was typical in late summer (August and September), with a high occurrence frequency (16.1%).

These mixing patterns (MIX7–9) appeared at similar discharge conditions, when the Maros contributed by ca. 20–50% to the discharge of the Tisza (mean $Q_{Makó}/Q_{Szeged}$: 0.31), and the slope difference between the two rivers was low (mean ΔS: −13.9 cm/km). The

highest discharge ratio (mean $Q_{Makó}/Q_{Szeged}$: 0.35), the lowest discharge difference (mean ΔQ: 170 m³/s), and the smallest slope difference (mean ΔS: −14.9 cm/km) occurred within the MIX9 pattern, referring to the fact that the high contribution from the Maros not only translated to a dominancy of MW but also the MIX's.

Within the class of dominance of MIX, the water of the Tisza or Maros could upwell forming the patterns MIX10 and MIX11 (Figure 8). In the case of the MIX10 pattern, the Tisza upwelled, similarly to the TW4 pattern: the TW was observed at S1, then it disappeared, and afterward, it reappeared between S2 and S4. However, the characteristic feature of MIX10 was that the TW seemed to be blocked by the MW, and not by the MIX, which was the case in the TW4 pattern. While the MW extended only between S1 and S2, it had a significant lateral extent (35–100%). Due to the upwelling of the Tisza water, the MIX could be observed between S2 and between S3 and S4, then it reappeared at the downstream end of the studied area (between S4 and S5), with a lateral extent range between 10 and 100%. The MIX10 pattern usually appeared during the summer (July and August), when the Maros had a higher contribution than the TW4 pattern, as the discharge ratio in MIX10 (mean $Q_{Makó}/Q_{Szeged}$: 0.25) was greater than its counterpart in TW4 (mean $Q_{Makó}/Q_{Szeged}$: 0.2); furthermore, the discharge, daily change and slope differences in MIX10 were lower (mean ΔQ: 223 m³/s; mean $\Delta H_{Algyő}$–$\Delta H_{Makó}$: −2.5 cm; mean ΔS: −13.7 cm/km) than their counterpart in TW4 (mean ΔQ: mean: 323 m³/s; mean $\Delta H_{Algyő}$–$\Delta H_{Makó}$: 4.4 cm; mean ΔS:−12.9 cm/km). The pattern MIX10 had greater frequency (12.6%) than the pattern TW4 (5.6%).

The MIX11 pattern represents (Table 4, Figure 8) the upwelling of the Maros with the dominancy of MIX; however, it was very unusual (frequency: 1.4%). This pattern was similar to the TW5 pattern in terms of the disappearance of MIX at the upstream part of the study area (S1–S2) and then reappearance downstream (MIX11: S3–S4; TW5: S3–S5). However, in MIX11, it interfered with the MIX water, not with the TW like TW5. Furthermore, it had less lateral extent (15–35%) than the TW5 (20–95%). The decrease of the areal coverage of MW in MIX11 was substituted by MIX, as the MIX covered greater area than in case of TW5 (S1–S5: 5–100%). The TW had a similar extent in both patterns, as it extended between S1 and S3 with an average lateral percentage of 60%. The MIX11 was observed in April and August, when the discharge ratio (mean $Q_{Makó}/Q_{Szeged}$: 0.25) was 1.25 times higher than TW5 (mean $Q_{Makó}/Q_{Szeged}$: 0.2). Moreover, the daily change and slope differences showed lower values in MIX11 (mean $\Delta H_{Algyő}$–$\Delta H_{Makó}$: −1.0 cm; mean ΔS: −13.0 cm/km) than in TW5 (mean $\Delta H_{Algyő}$–$\Delta H_{Makó}$: 4.7 cm; mean ΔS: −12.1 cm/km), which supported the high contribution of the Maros.

Comparing the mixing patterns with the hydrological parameters of the two rivers (Table 4, Figure 8), it could be noticed that usually, the TW dominated. The TW1–5 patterns developed when the Tisza had high stages and discharges, whereas the Maros had low stages and discharges, as the lowest average discharge ratio ($Q_{Makó}/Q_{Szeged}$: 0.16) existed within this pattern. Thus, the Tisza impounded the low-discharge Maros. On the other hand, the dominancy of the Maros (pattern MW6) usually occurred during high stages in both rivers, when the discharge ratio was very high (mean $Q_{Makó}/Q_{Szeged}$: 0.34); thus, the Maros supplied almost one-third of the water of the Tisza. Therefore, the Maros could penetrate the confluence zone deeper; however, due to the high stage of the Tisza, the MW could not extend laterally, but instead, it extended downstream until the end of the study area with a considerable areal coverage. The most common mixed pattern (MIX9) appeared in the confluence zone in late summer (August and September), when both rivers had low stages, and their discharge ratio was high (mean $Q_{Makó}/Q_{Szeged}$: 0.35), thus the Maros contributed considerably to the discharge of the Tisza, but the MW disappeared quickly due to the mixing process and converted into MIX with a significant area. The appearance of the waters of one of the rivers at the end of the study area (upwelling patterns: TW4–5 and MIX10–11) was not frequent. The upwelling of the Tisza (TW4 and MIX10) usually occurred in August, when both rives had low stages. Probably in these exceptional events, the Maros water stratified over the low velocity Tisza water because of its higher temperature, thus the MW covered almost the whole area at the point of the

confluence (S1–2: 35–100%); however, afterward, the Tisza water reappeared downstream (S2–4). The upwelling of the Maros (TW5 and MIX11) had the lowest probability; it usually occurred when the Tisza had high stages, and the Maros had low stages but with a high suspended load. As a result, the Tisza water stratified over the water of the Maros between S1 and S3, however the MW reappeared at the downstream part of the confluence (S3–S5).

3.5. Predictive Models

Predictive equations were produced for three groups of data: (1) all data considered; (2) cluster I (low and medium discharges) data considered; (3) cluster II (high discharges) data considered. Table 5 shows the produced equations for the three cases and the R^2 (coefficient of determination) for each model. The produced equations show the highest accuracy on the prediction of the areal distribution of TW (R^2: 0.6–0.63) and MW (R^2: 0.61–0.7), whereas the lowest accuracy can be observed with MIX (R^2: 0.4–0.55). The prediction of the longitudinal extent (L) of MW in the confluence area is the most reliable if it is based on the areal distribution (%) of MW (R^2: 0.64–0.82).

Table 5. Predictive equations for the areal distribution of the mixing waters (TW, MW, and MIX) and the longitudinal extent (L) of MW in the study area for the three groups of data.

Group of Data Considered	Model	R^2
All Data	$TW = 1076.84 − 87.55 (Q_{Makó}/Q_{Szeged}) + 0.048 (\Delta Q) − 12.96 (H_{Makó})$	0.63
	$MW = −750.23 + 0.25 (Q_{Makó}) − 0.09 (Q_{Szeged}) + 8.03 (S_{Tisza}) − 52.94 (Q_{Makó}/Q_{Szeged}) + 10.46 (H_{Szeged})$	0.62
	$MIX = 24.06 + 97.93 (Q_{Makó}/Q_{Szeged}) − 6.93 (S_{Tisza})$	0.55
	$Long.\ Ext. = −83357.44 + 1077.04 (H_{Makó}) − 4.56 (\Delta Q) + 940.93 (S_{Tisza})$	0.41
	$Long.\ Ext. = 97.92 (MW) − 4.61$	0.73
Cluster I ($Q_{Algyő}$: 747 m³/s; $Q_{Makó}$: 150 m³/s)	$TW = 14784.38 + 13.12 (S_{Maros}) − 190.83 (H_{Makó}) + 0.18 (Q_{Szeged}) + 0.94 (Q_{Makó})$	0.61
	$MW = 2658.90 + 0.44 (Q_{Makó}) − 33.99 (H_{Makó})$	0.61
	$MIX = 23.42 + 99.45 (Q_{Makó}/Q_{Szeged}) − 5.80 (S_{Tisza})$	0.40
	$Long.\ Ext. = 1374.5 + 23.97 (Q_{Makó}) − 5976.38 (Q_{Makó}/Q_{Szeged}) − 3.40 (\Delta Q)$	0.56
	$Long.\ Ext. = 108.26 (MW) − 256.7$	0.82
Cluster II ($Q_{Algyő}$: 747 m³/s; $Q_{Makó}$: 150 m³/s)	$TW = 117.51 − 284.14 (Q_{Makó}/Q_{Szeged})$	0.60
	$MW = 53.36 − 2.09 (\Delta S) + 0.20 (Q_{Makó}) − 0.06 (Q_{Szeged})$	0.70
	$MIX = −865.36 − 0.06 (\Delta Q) + 12.12 (H_{Szeged})$	0.40
	$Long.\ Ext. = 996.37 + 11246.43 (Q_{Makó}/Q_{Szeged}) − 1.5 (\Delta Q)$	0.53
	$Long.\ Ext. = 82.605 (MW) + 526.24$	0.64

4. Discussion

The mixing process in the confluence area of the Tisza and its tributary (the Maros) and its correlation with the hydrological parameters of both rivers were analyzed in detail based on 143 Sentinel-2 satellite images taken between July 2015 and May 2021.

4.1. Hydrological Background of the Mixing

Based on the calculated daily water stage changes, the Maros River demonstrated the greatest daily rising and falling stages throughout the studied period, which refers to a flashy regime with rapid flood waves (below or above bankfull level) and short inundation periods. However, within the studied 7 years, only two tiny floods were recorded. This result is in line with the long-term hydrological analysis [74], which revealed that on the Maros there is a dramatic decrease in floods. Between 1876 and 2011, it decreased from 22.1 days/year to 14.7 days/year, while within the studied period (2015–2021) only two floods appeared for 1–5 days/year. From the point of mixing, it is also important, that usually the Maros floods usually precede the Tisza's by 1–2 days, whereas the lowest

stages of the Maros are followed by 1–4 days of the Tiszas. During flood waves, both rivers carry a considerable amount of water; however, the highest discharge ratios were recorded during low stages: at these occasions, the Maros contributed to 24–35% of the discharge of the Tisza, as the main river had a significant drop in discharge and slope values. The Maros usually has a much higher slope (max: 13–16.5 cm/km) than the Tisza (max: 4–5 cm/km). However, during floods on the Tisza River, the Maros might be impounded; therefore, the water slope of the Maros decreases. Thus, our study could be applied for rivers which have characteristically different regimes; the tributary has a higher slope, more diverse stage, and discharge values. However, the main river can influence the mixing processes by its higher discharge and impoundment.

4.2. Temporal Changes in the Area of Waters with Various Origin

The areal distributions of TW and MIX are highly correlated (r = −0.91); moreover, they are closely related to water stages and discharges of both rivers. The proportion of TW increases during flood-waves on the Tisza, whereas the mixing water is dominant at low stages. The areal coverage of Maros water shows less sensitivity to water stages and discharges, as it shows low coverage both during low and very high stages; however, its highest area is observed at near bankfull stages. This behavior may be interpreted as the impoundment of the tributary by the main river during high stages, as the momentum of the main river overweighs its counterpart's; thus, it prevents the tributary from spreading in the confluence area. One exceptional event was recorded throughout the studied period when the tributary water (MW) showed a significant spread in the confluence area at over bankfull stages of both rivers (June 2020). At this time, the tributary was able to interact effectively with the main river due to its very high momentum, as the tributary had the highest water stage and discharge recorded within the studied period.

The study revealed that the discharge ratio of the two rivers has the greatest influence on the area of the various water types (TW, MW, and MIX). It is especially valid for the water of the main river (TW) and the mixed water (MIX), which have a strong correlation with the discharge ratio (r: −0.73 and r: 0.67, respectively). This result is in line with the findings of Best and Reid [11], who proved a strong positive correlation between the areal coverage of the separation zone and the discharge ratio between the tributary and the mainstream. Furthermore, the discharge difference between the main river (the Tisza at Algyő) and the tributary (Maros at Makó) and their slope difference show moderate to strong correlation with the areal distribution (%) of the water types. However, a better correlation was achieved when the data were separated into two groups, though the mixing characteristics remained similar, which was also confirmed by the HCA cluster analysis.

The Pearson correlation matrix revealed that, while the water of the main river (TW) and the mixed water (MIX) has high sensitivity to the hydrological situations in both rivers, the water of the tributary (MW) shows lower sensitivity to these parameters, as it is much more dependent just on the hydrological parameters of the tributary itself. This behavior is reflected by the mixing process too, as it seems in most cases the tributary with its high concentration of suspended sediment rapidly disappears in the confluence area, and it can keep its high suspended sediment concentration just in rare cases. On the other side, there is a robust variation in the hydrological conditions in the rivers, which does not match with the temporal variation of the water of the tributary (MW).

4.3. Mixing Patterns

Based on the lateral and longitudinal extensions of the three identified water classes (TW, MW, and MIX), 11 mixing patterns were identified, which depend on the hydrological characteristics and momentum of both rivers. The characteristic periods of each mixing pattern were revealed, similarly to the analysis of the confluence of the Solimões and Negro Rivers [48,49].

The water of the main river (TW1 pattern) usually dominates during its high stages and simultaneous low stages in the tributary (usually in early winter and early spring).

However, it could also dominate during high stages in both rivers (TW2 pattern: high coverage of the tributary's water) and very less common during low stages in both rivers (TW3 pattern: high coverage of the mixed water). The tributary water usually dominates during high stages in both rivers (MW6 pattern), or high stages in the tributary and low stages in the main river during spring and the summer months. In these cases, the higher slope of the tributary creates favorable conditions for the appearance of the tributary's water without considerable mixing with the main river. The considerable mixing of the waters (MIX7–9 pattern) usually is the most common during low stages in both rivers (usually late summer and early autumn), or during high stages in both rivers, or medium stages in the tributary and low stages in the main river, thus in cases when the flow conditions of the joining rivers are similar. The fact that in the confluence area of the Tisza and Maros Rivers, the mixing water can dominate during low stages and that the lowest coverage of MIX water was observed during a flood contradict the results of *Park and Latrubess*e [49], who concluded that high water mixture usually occurs during floods. The differences between the studies could be explained by (1) the low slope of the Tisza and Maros rivers even during floods and (2) the relatively high confluence angle. These can result in the impoundment; thus, the impounded river is almost blocked by the dominant river. Thus, limited mixing can happen.

There are some exceptional events when the water of the Tisza (TW4 and MIX10) or the Maros (TW5 and MIX11) upwells; thus, their water appears in the downstream end of the confluence area. It could be explained by the different densities of the joining waters, related to the considerable difference between their suspended sediment concentration or their water temperature. These upwelling patterns usually occur during summer or autumn low stages, when the temperature conditions of the joining rivers are very different. As the Maros is very shallow (3.5–5.5 m), at the beginning or the end of summer, its water can be much warmer or colder than the deep Tisza's (10–20 m). As a result, the water of one of the rivers stratifies above the other; thus, due to the spiral flow, the other water appears (upwells) just at the downstream end of the confluence area.

4.4. Support for Future Sediment Sampling

The mixing pattern should be known if someone plans a sampling campaign (i.e., for sediment, pollutant, microplastic, phytoplankton) in a confluence area. The analysis based on the collected samples without knowing the mixing pattern might lead to misinterpretations and wrong conclusions, as the joining waters might have very different sediment characteristics, and their mixing is dependent on various parameters. Therefore, predictive equations for the areal distribution of the mixing waters and their longitudinal extent in the confluence area can be helpful when planning a sediment sampling. In our case, by applying the created equations, anyone can predict the areal distribution (%) of the waters in the confluence (TW, MW, MIX) and the longitudinal extent (L) of the tributary's water based on the actual hydrological parameters measured at the three neighboring gauging stations (Algyő, Szeged, and Makó). Thus, the near-future mixing could be predicted, and the sampling campaign could be carefully planned.

The accuracy of the derived equations could be rated as moderate to good. No better accuracy was achieved because of the complexity of the mixing process: it is not only dependent on the hydrological parameters, but also other driving factors, such as the morphological characteristics of the channels, temporal dynamism of the sandy channel, temporal change of the transported suspended sediment load, and water temperature conditions of both rivers.

4.5. The Applicability of the Unsupervised Classification Method

The K-means unsupervised classification algorithm proved its ability as a good tool to study the mixing process in confluences. Its application supported the identification of pixels representing the water of the main river, the tributary, and their mixture. The reason behind this is that there are significant differences between the suspended sediment concentrations between the joining rivers [2,7,20,22,38,41], which contrasted the water-color considerably; and in turn, the reflectance values for the three classes were clearly separated by the unsupervised technique. Fortunately, most confluences have the same feature of watercolor difference; thus, we recommend this technique during the analysis of the mixing process in confluences. It is especially a useful method, as it is often difficult to collect water samples to calibrate satellite images for supervised classification.

5. Conclusions

River confluences are considered as turning spots along streams, as they affect not only the water flowing downstream but also the sediment and pollutant concentrations. The mixing process in the confluence area is very complex, as it is influenced by many factors related to the morphological characteristics, hydrological and sediment transport conditions of the joining rivers. The mixing process is even more complex if one considers that the above-mentioned parameters can change in time and are relative to each other at the two joining rivers.

The impacts of the various hydrological parameters on the spatio-temporal dynamism of mixing in the Tisza and Maros Rivers confluence were investigated using Sentinel-2 satellite images, applying K-means unsupervised classification technique. The mixing pattern was analyzed based on 143 images covering the period between July 2015 and May 2021. The areal distribution of the water originated from the Tisza (TW), the joining Maros (MW), and their mixture (MIX) were compared with the hydrological parameters of the joining rivers.

It was concluded that the water areas of the main river (TW) and the mixed water (MIX) are highly correlated to the water stage in both rivers. However, the area of the water of the tributary (MW) showed a weaker relationship, as it showed a negative correlation with the stages above the bankfull level and a positive correlation with the stages below this level, which could happen due to the impoundment of the tributary by the main river during floods. The lateral extents of the three water types followed also the same temporal change as the areal coverage. Despite the complexity of the mixing process in the confluence area due to the various driving factors, it can be concluded that the hydrological parameters have a significant impact on the mixing process; therefore, they could be used to predict the mixing pattern in the confluence area. The discharge ratio between both rivers gives the best representation of the mixing process, especially for the areal percentages of the water of the main river and the mixed water.

Based on the large number of Sentinel-2 satellite images altogether, 11 mixing patterns were identified. Usually, the water of the main river (TW) dominates the confluence area. It has almost complete coverage in January and November (TW1 pattern) when the main river has high stages, and the tributary has low waters. The water of the tributary (MW) can dominate just in June or July when the water stages in both rivers are high, but the tributary has a much greater slope. The mixing of the two rivers is considerable when they have similar hydrological conditions, and none of them dominates over the other. The upwelling of one of the waters at the downstream end of the confluence area is not rare, and it is in connection with the considerably different density conditions of the joining streams.

The identified mixing patterns appear in distinct periods. Therefore, collecting water samples just from one point in the confluence area can lead to errors, as at a given point, the water has a different origin in the various months. Therefore, in the confluence area, sampling from several points is suggested. However, it also must be noted that various

mixing patterns (upwelling, from no-mixing to almost total mixing) alternate within a year, and even at the most downstream cross section of the study area, thus in 26 times of the Tisza's channel width (w) no complete mixing was achieved. It may take 15–150 km for complete mixing according to the assumption of *Jirka* [21]. Therefore, we suggest to avoid the confluence area during sampling; or carefully analyze the mixing pattern during sampling to evade misinterpretations.

Appendix A

The Figures A1–A3 and their descriptions are included in the Appendix A.

Figure A1: The maximum rising (145 cm/day) and falling (−151 cm/day) rates were recorded on the Maros at Makó during February 2017 flood. On the other hand, the fastest rising on the Tisza was only 113 cm/day (at Algyő) and 94 cm/day (at Szeged) during the flood in January 2016. The rapidest falling stage (−81 cm/day at Algyő and −74 cm/day at Szeged) was detected during the end of the flood in June 2019. The greatest differences in the daily change of water stage between the Tisza and Maros rivers (>80 cm) were observed during floods (November 2015, January 2016, and February 2017); however, apart from these periods, the differences between the two rivers fluctuated steadily.

Figure A2: Heat maps were created based on the lateral percentages of Tisza water (TW), Maros water (MW), and their mixture (MIX) at the five studied cross sections. The water of the main river (TW) usually dominated the confluence area. In most cases (75%) in the first (S1) cross section (just 110 m downstream of the confluence), the Tisza water occupied 15–68% of the cross section. In some cases (2%), the mixing was a minor process, thus along all 5 cross sections the TW dominated (Figure A2A). It happened in the late autumn and winter months (e.g., from November 2015 until January 2016). An almost similar situation evolved (in 13% of the cases) when the TW dominated four cross sections (S2–5), and only in the first (S1) cross section was its proportion below 90%. In the rest of the cases (10%) high contribution of the TW was detected just at the downstream cross sections (S3–5) as if the TW was "upwelling" 2.3–4.1 km far from the confluence. This could happen at any time of the year, but it was common in summer and late autumn.

The Maros water (MW) showed fewer spatio-temporal variations between the five cross sections (Figure A2B). Almost in every case (99%), the proportion of MW was the highest (10–61%) at the upstream S1 cross section. Additionally, at this cross section, about 5% of cases the Maros water occupied a greater proportion of the channel (38–61%) than the TW (15–47%), despite the fact that the Tisza channel is 103 m wide at the confluence, while the Maros is only 70 m. In most (92%) cases, the MW quickly disappeared, so in the downstream cross sections (S2–5), its average proportion was 30%. In the last case (3%), the MW was detectable even at the S4–S5 cross sections with high areal coverage, as sometimes the "upwelling" MW had a higher proportion (30–100%) than at the upstream cross sections. This case was common from April to mid-August, and for example, this situation dominated the summer in 2016. The measured lateral percentages of MW at the five cross

sections and the calculated areal percentages of MW in the entire confluence had similar temporal patterns throughout the studied period.
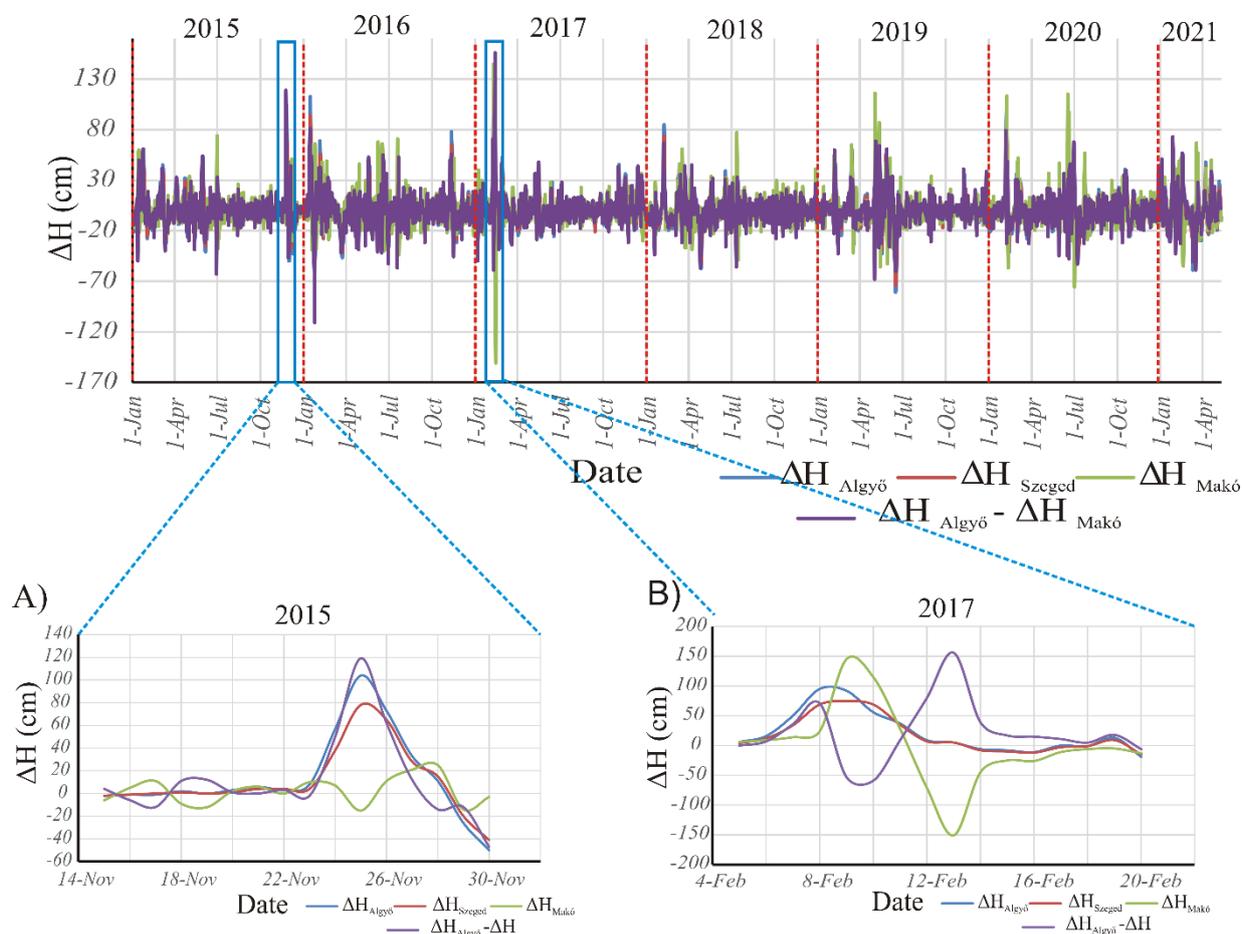

Figure A1. Calculated daily water stage change (cm/day) at the three gauging stations (Algyő, Szeged, and Makó), and the daily difference change between Algyő and Makó throughout the studied period (January 2015-May 2021). Zooming into flood events in November 2015 (**A**) and February 2017 (**B**), as an example of the greatest daily differences.

The mixed water (MIX) of the two rivers showed high spatio-temporal variations between the five cross sections (Figure A2C). Almost in all cases (99%), the MIX had a very low proportion (2–28%) in the first cross section (S1), as its proportion increased gradually from S1 towards S5. Considering all studied dates, in 17% of cases, no mixing was observed along the five cross sections due to the dominancy of water from one of the joining rivers (usually the Tisza). This case usually occurred in the late autumn and winter months (e.g., from November until January). In 34% of cases, the MIX had very high coverage (>85%) between S4 and S5; however, the significant coverage of MIX between S2 and S5 was observed only in 3% of cases. This significant coverage between S2 and S5 usually occurred in spring and summer (e.g., April and August). In the last case (11%), the MIX almost disappeared or was recorded with very low coverage (0–15%) at S4; however, it appeared again after this section with a significant coverage (>80%) at S5. This case was related to the upwelling of the Tisza or Maros water at the downstream part of the study area (between S4 and S5). This case was observed in early summer (May) or late autumn (September–November).
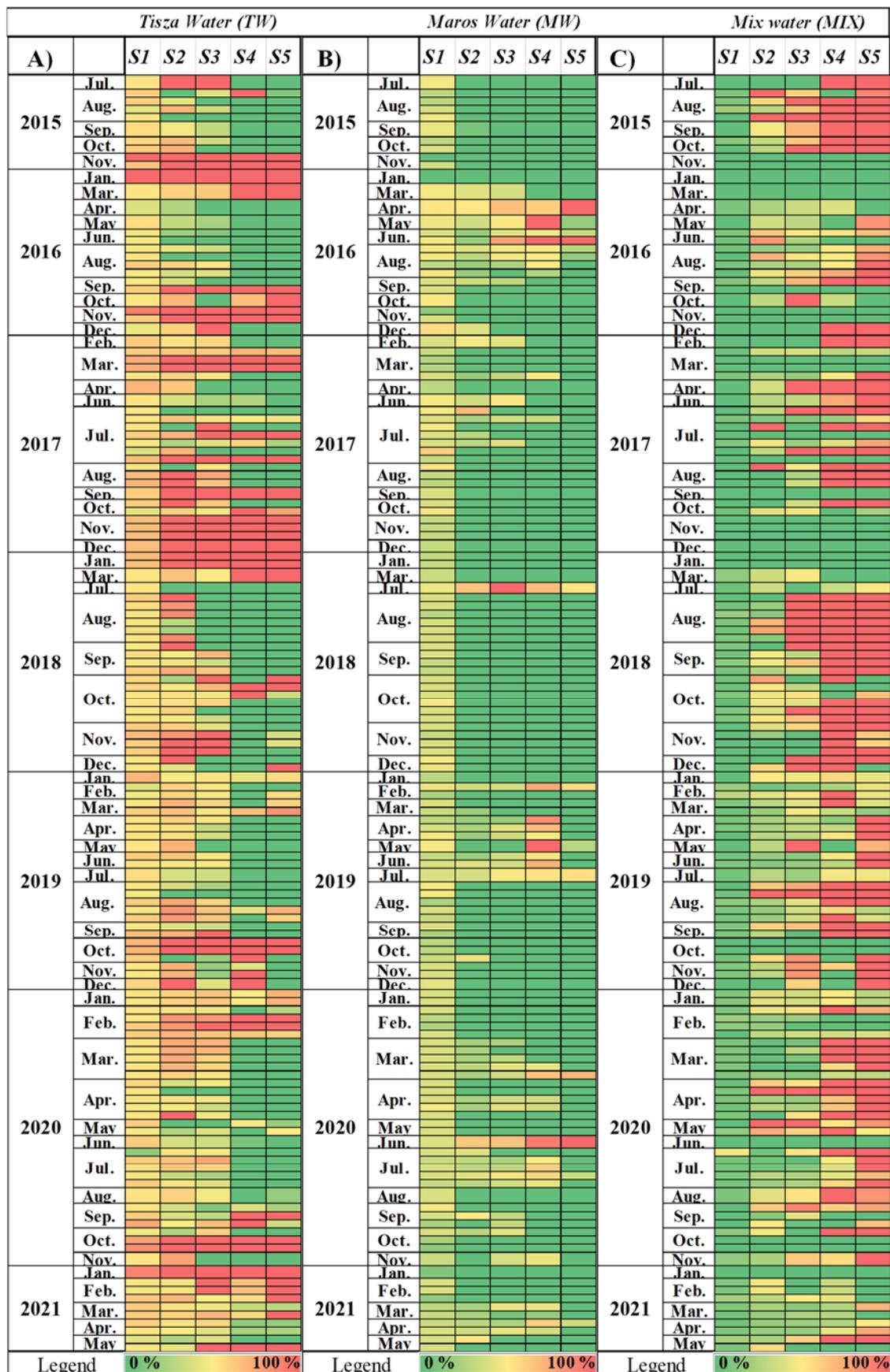
Figure A2. Heat maps of the lateral percentages of (**A**) Tisza water (TW), (**B**) Maros water (MW) and (**C**) their mixture (MIX) at the five cross sections. Each row represents one date, when a Sentinel-2 image was analyzed.

Figure A3: The areal distributions of the various waters and the actual hydrological parameters were compared (Figure A3) to understand the driving factors of the mixing. The discharge ratio of the two rivers gives the best representation of the areal percentages of TW, MW, and MIX, as it correlated positively with the areal percentage of MW, and MIX, and negatively with the TW percentage (Figure A3A). The discharge and slope differences showed good correlations as well, but less than the discharge difference (Figure A3B,C). In contrast, the differences in daily stage change showed no correlation with the areal percentages of water types (Figure A3D); therefore, this parameter had the lowest impact on the mixing of water with various origins.
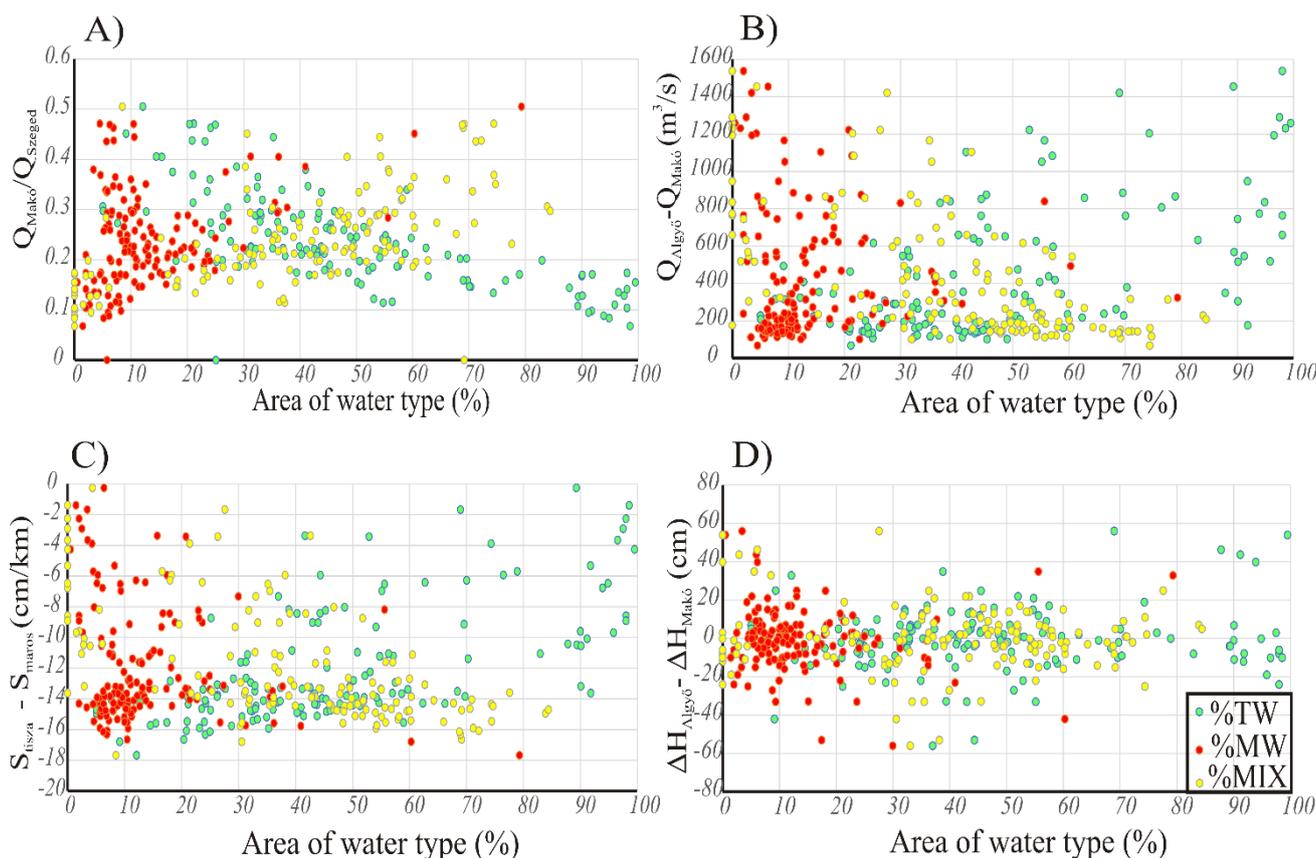

Figure A3. The relationship between the areal percentages of Tisza water (TW), Maros water (MW) and mixture (MIX) and the ratios and differences between the hydrological parameters in both rivers. (**A**) Ratio between the discharge values of the Maros and Tisza Rivers ($Q_{Makó}/Q_{Szeged}$). (**B**) Absolute discharge difference of the two rivers measured before the confluence ($Q_{Algyő}-Q_{Makó}$). (**C**) Slope difference between the two rivers (ΔS). (**D**) Difference in daily water level changes of the two rivers ($\Delta H_{Algyő}-\Delta H_{Makó}$).

References

1. Bilal, A.; Xie, Q.; Zhai, Y. Flow, Sediment, and Morpho-Dynamics of River Confluence in Tidal and Non-Tidal Environments. *J. Mar. Sci. Eng.* **2020**, *8*, 591.
2. Rice, S.; Roy, A.; Rhoads, B. *River Confluences, Tributaries and the Fluvial Network*. JohnWiley & Sons Ltd, England, UK, 2008.
3. Wuppukondur, A.; Chandra, V. Mitigate Reservoir Sedimation by Reducing Scour at River Confluence: An experimantal Study. In Proceedings of the 8th International Perspective on Water Resources and the Environment, Colombo, Sri Lanka, 4–6 January 2016.
4. Boyer, C.; Roy, A.G.; Best, J.L. Dynamics of a river channel confluence with discordant beds: Flow turbulence, bed load sediment transport, and bed morphology. *J. Geophys. Res. Earth Surf.* **2006**, *111*, F04007.
5. Amini, N.; Balouchi, B.; Bejestan, M.S. Reduction of local scour at river confluences using a collar. *Int. J. Sediment. Res.* **2017**, *32*, 364–372.
6. Best, J.L. Flow dynamics at river channel confluences: Implications for sediment transport and bed morphology. *Soc. Econ. Paleontol. Mineral. (SEPM)* 1987.

7. Unde, M.G.; Dhakal, S. Sediment characteristics at river confluences: A case study of the Mula-Kas confluence, Maharashtra, India. *Prog. Phys. Geogr.* **2009**, *33*, 208–223.

8. Ashmore, P.; Ferguson, R.; Prestegaard, K.; Ashworth, P.; Paola, C. Secondary flow in anabranch confluences of a braided, gravel-bed stream. *Earth Surf. Process. Landf.* **1992**, *17*, 299–311.

9. Rhoads, B.L.; Riley, J.D.; Mayer, D.R. Response of bed morphology and bed material texture to hydrological conditions at an asymmetrical stream confluence. *Geomorphology* **2009**, *109*, 161–173.

10. Yuan, S.; Tang, H.; Xiao, Y.; Qiu, X.; Xia, Y. Water flow and sediment transport at open-channel confluences: An experimental study. *J. Hydraul. Res.* **2018**, *56*, 333–350.

11. Best, J.L.; Reid, I. Separation zone at open-channel junctions. *J. Hydraul. Eng.* **1984**, *110*, 1588–1594.

12. Cushman-Roisin, B.; Constantinescu, G.S. Dynamical adjustment of two streams past their confluence. *J. Hydraul. Res.* **2020**, *58*, 305–313.

13. Guillén-Ludeña, S.; Franca, M.; Cardoso, A.; Schleiss, A. Evolution of the hydromorphodynamics of mountain river confluences for varying discharge ratios and junction angles. *Geomorphology* **2016**, *255*, 1–15.

14. Constantinescu, G.; Miyawaki, S.; Rhoads, B.; Sukhodolov, A. Numerical analysis of the effect of momentum ratio on the dynamics and sediment-entrainment capacity of coherent flow structures at a stream confluence. *J. Geophys. Res. Earth Surf.* **2012**, *117*.F04028.

15. Best, J.L. Sediment transport and bed morphology at river channel confluences. *Sedimentology* **1988**, *35*, 481–498.

16. Roy, A.; Bergeron, N. Flow and particle paths at a natural river confluence with coarse bed material. *Geomorphology* **1990**, *3*, 99–112.

17. Rhoads, B.L. Mean structure of transport-effective flows at an asymmetrical confluence when the main stream is dominant. *Coherent Flow Struct. Open Channels* **1996**, 18, 491–517.

18. Singh, U.K.; Ahmad, Z.; Kumar, A.; Pandey, M. Incipient motion for gravel particles in cohesionless sediment mixtures. *Iran. J. Sci. Technol. Trans. Civ. Eng.* **2019**, *43*, 253–262.

19. Smith, R.; Daish, N. Dispersion far downstream of a river junction. *Phys. Fluids A: Fluid Dyn.* **1991**, *3*, 1102–1109.

20. Mackay, J.R. Lateral mixing of the Liard and Mackenzie rivers downstream from their confluence. *Can. J. Earth Sci.* **1970**, *7*, 111-124.

21. Jirka, G.H. Mixing and dispersion in rivers.In *River Flow*; AA Balkema Publishers: London, UK, 2004; pp. 13–27.

22. Ghosh, K.G. Sediment transport at the river confluences: Few observations from a sub-tropical plateau fringe river of eastern India. *Geol. Ecol. Landsc.* **2020**, 1–24, doi:10.1080/24749508.2020.1752501.

23. Park, J.; Batalla, R.J.; Birgand, F.; Esteves, M.; Gentile, F.; Harrington, J.R.; Navratil, O.; López-Tarazón, J.A.; Vericat, D. Influences of catchment and river channel characteristics on the magnitude and dynamics of storage and re-suspension of fine sediments in river beds. *Water* **2019**, *11*, 878.

24. Guyot, J.-L.; Filizola, N.; Guimarães, V. Amazon suspended sediment yield measurements using an Acoustic Doppler Current Profiler (ADCP): First results. *Hydrol. Humid Trop. Environ. Int. Symp. AHS-AISH Publ.* **1998**, 253, 109–115.

25. Ahmed, I.; Pan, N.D.; Debnath, J. A study on suspeded sediment discharge and bed load grain size of the Gumti River of Tripura at some selected tributary confluence points. *Int. J. Geol. Earth Environ. Sci.* **2016**, *6*, 43–53.

26. Pu, J.H.; Wallwork, J.T.; Khan, M.; Pandey, M.; Pourshahbaz, H.; Satyanaga, A.; Hanmaiahgari, P.R.; Gough, T. Flood suspended sediment transport: Combined modelling from dilute to hyper-concentrated flow. *Water* **2021**, *13*, 379.

27. Lepesqueur, J.; Hostache, R.; Martínez-Carreras, N.; Montargès-Pelletier, E.; Hissler, C. Sediment transport modelling in riverine environments: On the importance of grain-size distribution, sediment density, and suspended sediment concentrations at the upstream boundary. *Hydrol. Earth Syst. Sci.* **2019**, *23*, 3901–3915.

28. Lavery, P.; Pattiaratchi, C.; Wyllie, A.; Hick, P. Water quality monitoring in estuarine waters using the Landsat Thematic Mapper. *Remote. Sens. Environ.* **1993**, *46*, 268–280.

29. Liu, Y.; Islam, M.A.; Gao, J. Quantification of shallow water quality parameters by means of remote sensing. *Prog. Phys. Geogr.* **2003**, *27*, 24–43.

30. Ritchie, J.C.; Zimba, P.V.; Everitt, J.H. Remote sensing techniques to assess water quality. *Photogramm. Eng. Remote. Sens.* **2003**, *69*, 695–704.

31. Zhou, Y.; Zhou, W.Q.; Wang, S.X.; Zhang, P. Applications of remote sensing techniques to inland water quality monitoring. *Adv. Water Sci.* **2004**, *15*, 312–317.

32. Alparslan, E.; Aydöner, C.; Tufekci, V.; Tüfekci, H. Water quality assessment at Ömerli Dam using remote sensing techniques. *Environ. Monit. Assess.* **2007**, *135*, 391–398.

33. Chen, Q.; Zhang, Y.; Hallikainen, M. Water quality monitoring using remote sensing in support of the EU water framework directive (WFD): A case study in the Gulf of Finland. *Environ. Monit. Assess.* **2007**, *124*, 157–166.

34. He, W.; Chen, S.; Liu, X.; Chen, J. Water quality monitoring in a slightly-polluted inland water body through remote sensing—Case study of the Guanting Reservoir in Beijing, China. *Front. Environ. Sci. Eng. China* **2008**, *2*, 163–171.

35. Usali, N.; Ismail, M.H. Use of remote sensing and GIS in monitoring water quality. *J. Sustain. Dev.* **2010**, *3*, 228.

36. Chebud, Y.; Naja, G.M.; Rivero, R.G.; Melesse, A.M. Water quality monitoring using remote sensing and an artificial neural network. *Water Air Soil Pollut.* **2012**, *223*, 4875–4887.

37. Mohsen, A.; Elshemy, M.; Zeidan, B. Water quality monitoring of Lake Burullus (Egypt) using Landsat satellite imageries. *Environ. Sci. Pollut. Res.* **2021**, *28*, 15687–15700.

38. Gernez, P.; Lafon, V.; Lerouxel, A.; Curti, C.; Lubac, B.; Cerisier, S.; Barillé, L. Toward Sentinel-2 high resolution remote sensing of suspended particulate matter in very turbid waters: SPOT4 (Take5) Experiment in the Loire and Gironde Estuaries. *Remote. Sens.* **2015**, *7*, 9507–9528.

39. Li, D.; Wang, G.; Qin, C.; Wu, B. River Extraction under Bankfull Discharge Conditions Based on Sentinel-2 Imagery and DEM Data. *Remote. Sens.* **2021**, *13*, 2650.

40. Maurice-Bourgoin, L.; Quemerais, B.; Moreira-Turcq, P.; Seyler, P. Transport, distribution and speciation of mercury in the Amazon River at the confluence of black and white waters of the Negro and Solimoes Rivers. *Hydrol. Process.* **2003**, *17*, 1405–1417.

41. Lane, S.N.; Parsons, D.R.; Best, J.L.; Orfeo, O.; Kostaschuk, R.; Hardy, R.J. Causes of rapid mixing at a junction of two large rivers: Río Paraná and Río Paraguay, Argentina. *J. Geophys. Res. Earth Surf.* **2008**, *113*, F02024.

42. Gaudet, J.M.; Roy, A.G. Effect of bed morphology on flow mixing length at river confluences. *Nature* **1995**, *373*, 138–139.

43. Park, E.; Latrubesse, E.M. Modeling suspended sediment distribution patterns of the Amazon River using MODIS data. *Remote. Sens. Environ.* **2014**, *147*, 232–242.

44. Pham, Q.V.; Ha, N.T.T.; Pahlevan, N.; Oanh, L.T.; Nguyen, T.B.; Nguyen, N.T. Using Landsat-8 images for quantifying suspended sediment concentration in Red River (Northern Vietnam). *Remote. Sens.* **2018**, *10*, 1841.

45. Cremon, É.H.; da Silva, A.M.S.; Montanher, O.C. Estimating the suspended sediment concentration from TM/Landsat-5 images for the Araguaia River—Brazil. *Remote. Sens. Lett.* **2020**, *11*, 47–56.

46. Doxaran, D.; Froidefond, J.-M.; Castaing, P. Remote-sensing reflectance of turbid sediment-dominated waters. Reduction of sediment type variations and changing illumination conditions effects by use of reflectance ratios. *Appl. Opt.* **2003**, *42*, 2623–2634.

47. Umar, M.; Rhoads, B.L.; Greenberg, J. Use of multispectral satellite remote sensing to assess mixing of suspended sediment downstream of large river confluences. *J. Hydrol.* **2018**, *556*, 325–338.

48. Marinho, T.; Filizola, N.; Martinez, J.-M.; Armijos, E.; Nascimento, A. Suspended sediment variability at the Solimões and Negro confluence between May 2013 and February 2014. *Geosciences* **2018**, *8*, 265.

49. Park, E.; Latrubesse, E.M. Surface water types and sediment distribution patterns at the confluence of mega rivers: The Solimões-Amazon and Negro Rivers junction. *Water Resour. Res.* **2015**, *51*, 6197–6213.

50. Sipos, G.; Kiss, T.; Fiala, K. Morphological alterations due to channelization along the lower Tisza and Maros Rivers (Hungary). *Geogr. Fiscicae Din. Quat.* **2007**, *30*, 239–247.

51. Kiss, T.; Fiala, K.; Sipos, G. Alterations of channel parameters in response to river regulation works since 1840 on the Lower Tisza River (Hungary). *Geomorphology* **2008**, *98*, 96–110.

52. Kiss, T.; Fiala, K.; Sipos, G.; Szatmári, G. Long-term hydrological changes after various river regulation measures: Are we responsible for flow extremes? *Hydrol. Res.* **2019**, *50*, 417–430.

53. Sipos, G.; Kiss, T.; Oroszi, V. Geomorphological Process Along the Lowland Sections of the Maros/Mures and Kôrôs/CRIS Rivers. *Ecol. Soc-Econ. Relat. Val. River Kôrôs/Cris. River Maros/Mure* **2011**, 35.

54. Amissah, G.J.; Kiss, T.; Fiala, K. Morphological evolution of the lower Tisza River (Hungary) in the 20th century in response to human interventions. *Water* **2018**, *10*, 884.

55. Bogárdi, J. *Sediment Transport in Alluvial Streams*; Akademiai Kiado Budapest: Budapest, Hungary, 1974.

56. Reizner, J. Szeged Története. Available online: http://www.bibl.u-szeged.hu/reizner/index2.html 1900.(accessed on 6 November 2021). (In Hungarian)

57. Laczai, I.A. Maros szabályozása és kanyarulati viszonyai. In *Maros Vízrajzi Atlasz*; VITUKI: Budapest, Hungary, 1975; pp. 20–24. (In Hungarian)

58. Török, I. A Maros alföldi szakaszának szabályozási terve (0–51, 33 fkm). In *Regulation Plan Of The Lowland Section of River Maros*; *ATIVIZIG*: Szeged,Hungary, 1977. (In Hungarian)

59. SNAP(ESA). Available online: https://step.esa.int/main/download/snap-download/ (accessed on 20 June 2021).

60. Revel, C.; Lonjou, V.; Marcq, S.; Desjardins, C.; Fougnie, B.; Coppolani-Delle Luche, C.; Guilleminot, N.; Lacamp, A.-S.; Lourme, E.; Miquel, C.J.E.J.o.R.S. Sentinel-2A and 2B absolute calibration monitoring. *Eur. J. Remote. Sens.* **2019**, *52*, 122–137.

61. ESA, V.B.; Szantoi, Z.; Gascon, F. Copernicus Sentinel-2 Mission: Calibration and Validation activities. *GSICS Q.* **2020**, *14*, 1 doi:10.25923/enp8–6w06.

62. Drusch, M.; Del Bello, U.; Carlier, S.; Colin, O.; Fernandez, V.; Gascon, F.; Hoersch, B.; Isola, C.; Laberinti, P.; Martimort, P. Sentinel-2: ESA's optical high-resolution mission for GMES operational services. *Remote. Sens. Environ.* **2012**, *120*, 25–36.

63. Louis, J.; Debaecker, V.; Pflug, B.; Main-Knorn, M.; Bieniarz, J.; Mueller-Wilm, U.; Cadau, E.; Gascon, F. Sentinel-2 sen2cor: L2a processor for users. In Proceedings of the Living Planet Symposium, Prague, Czech Republik, 9–13 May 2016; pp. 1–8.

64. McFeeters, S.K. The use of the Normalized Difference Water Index (NDWI) in the delineation of open water features. *Int. J. Remote. Sens.* **1996**, *17*, 1425–1432.

65. Lloyd, S. Least squares quantization in PCM. *IEEE Trans. Inf. Theory* **1982**, *28*, 129–137.

66. Likas, A.; Vlassis, N.; Verbeek, J. The global k-means clustering algorithm. *Pattern Recognit.* **2003**, *36*, 451–461.

67. Ament, R.; Clevenger, A.P.; Yu, O.; Hardy, A. An assessment of road impacts on wildlife populations in US National Parks. *Environ. Manag.* **2008**, *42*, 480.

68. Dekker, A.G.; Vos, R.; Peters, S. Analytical algorithms for lake water TSM estimation for retrospective analyses of TM and SPOT sensor data. *Int. J. Remote. Sens.* **2002**, *23*, 15–35.

69. Doxaran, D.; Cherukuru, N.; Lavender, S.J. Apparent and inherent optical properties of turbid estuarine waters: Measurements, empirical quantification relationships, and modeling. *Appl. Opt.* **2006**, *45*, 2310–2324.

70. Tyler, A.; Svab, E.; Preston, T.; Presing, M.; Kovacs, W. Remote sensing of the water quality of shallow lakes: A mixture modelling approach to quantifying phytoplankton in water characterized by high-suspended sediment. *Int. J. Remote. Sens.* **2006**, *27*, 1521–1537.

71. Akoglu, H. User's guide to correlation coefficients. *Turk. J. Emerg. Med.* **2018**, *18*, 91–93.

72. Ward, J.H., Jr. Hierarchical grouping to optimize an objective function. *J. Am. Stat. Assoc.* **1963**, *58*, 236–244.

73. IBM SPSS. Available online: https://www.ibm.com/analytics/us/en/technology/spss/ (accessed on 25 May 2021).

74. Kiss, T.; Nagy, Z.; Balogh, M. Floodplain level development induced by human activity-case study in the lower Maros/Mures river, Romania and Hungary. *Carpathian J. Earth Environ. Sci.* **2017**, *12*, 83–93.